Agricultural and Forest Meteorology 342 (2023) 109692

Contents lists available at ScienceDirect

Agricultural and Forest Meteorology

journal homepage: www.elsevier.com/locate/agrformet

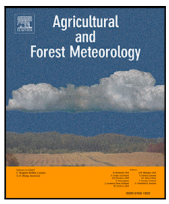

Merging flux-variance with surface renewal methods in the roughness sublayer and the atmospheric surface layer

Milan Fischer [a,b,*], Gabriel Katul [c], Asko Noormets [d], Gabriela Pozníková [a,b], Jean-Christophe Domec [e,f], Matěj Orság [a,b], Zdeněk Žalud [a,b], Miroslav Trnka [a,b], John S. King [g]

[a] Global Change Research Institute of the Czech Academy of Sciences, Bělidla 986/4a, Brno, 603 00, Czech Republic
[b] Department of Agrosystems and Bioclimatology, Faculty of Agronomy, Mendel University in Brno, Zemědělská 1, Brno, 613 00, Czech Republic
[c] Department of Civil and Environmental Engineering, Box 90287, Duke University, Durham, 27708-0287, NC, USA
[d] Department of Ecology and Conservation Biology, Texas A&M University, College Station, 77843-2138, TX, USA
[e] Bordeaux Sciences Agro, UMR INRAE ISPA 1391, Gradignan, 33175, France
[f] Nicholas School of the Environment, Box Box 90328, Duke University, Durham, 27708-0328, NC, USA
[g] Department of Forestry and Environmental Resources, Box 8008, North Carolina State University, Raleigh, 27695, NC, USA

ARTICLE INFO

Keywords:
Eddy covariance
Ramp-cliff temperature pattern
Sensible heat flux
Similarity theory
Surface renewal theory

ABSTRACT

Two micrometeorological methods utilizing high-frequency sampled air temperature were tested against eddy covariance (EC) sensible heat flux (H) measurements at three sites representing agricultural, agro-forestry, and forestry systems. The two methods cover conventional and newly proposed forms of the flux-variance (FV) and surface renewal (SR) schemes of differing complexities. The sites represent measurements in surface, roughness, and roughness to surface transitional layers. Regression analyzes against EC show that the most reliable FV and SR forms estimate H with slopes within ±10% from unity and coefficient of determination R^2>0.9 across all the three sites. The best performance of both FV and SR was found at the agricultural site with measurements well within the surface layer, while the worst was found for the tall forest with measurements within the roughness sublayer where its thickness needed to be additionally estimated. The main variable driving H in FV is the temperature variance, whereas in SR, it is the geometry of ramp-like structures. Since these structures are also responsible for most of the temperature variance, a novel FV-SR approach emerging from combining the methods is proposed and evaluated against EC measurements and conventional FV and SR schemes. The proposed FV-SR approach requiring only a single fast response thermocouple is potentially independent of calibration and ameliorates some of the theoretical objections that arise when combining ramp statistics with similarity arguments. The combination of methods also provides new insights into the contribution of coherent structures to the temperature variance and its dependence on atmospheric stratification. Other potential utility of the new method is to include it in multi-tool assessments of surface energy fluxes, since a convergence or divergence of the results has a high diagnostic value.

1. Introduction

While the significance of surface turbulent energy fluxes to agriculture and forestry are undisputed, robust approaches for their long-term monitoring remain a subject of inquiry. The eddy covariance (EC) method has become the 'gold standard' and is widely used nowadays for determining fluxes of latent (LE, W m^{-2}) and sensible (H, W m^{-2}) heat Aubinet et al. (1999), Foken (2008a). However, alternative approaches to EC often need to be considered (Kustas et al., 1994; Drexler et al., 2004; Pozníková et al., 2018) depending on costs and site considerations. From the less expensive end of the micrometeorological methods spectrum, the alternatives are represented by flux-variance (FV) and surface renewal (SR), followed by more traditional techniques such as the Bowen ratio and energy balance (BREB), and aerodynamic methods (Shuttleworth, 2007). Both BREB and aerodynamic methods require accurate measurements of vertical differences of mean air temperature and water vapor concentration, which poses a challenge especially above aerodynamically rough surfaces such as tall forests. Above such aerodynamically rough surfaces, vertical gradients of mean water vapor concentration or air temperature are generally small, necessitating large vertical separation of the instruments (Foken, 2008a; Lindroth and Halldin, 1990). In addition, the Monin and Obukhov (1954) similarity theory (MOST) involved in the aerodynamic method

* Corresponding author at: Global Change Research Institute of the Czech Academy of Sciences, Bělidla 986/4a, Brno, 603 00, Czech Republic.
E-mail address: fischer.m@czechglobe.cz (M. Fischer).

https://doi.org/10.1016/j.agrformet.2023.109692
Received 8 May 2023; Received in revised form 17 August 2023; Accepted 28 August 2023
Available online 8 September 2023

is valid only within the surface layer that is located some 2–3 h (Brunet, 2020), where h is the canopy height (m). In terrestrial systems, the upper end of the surface layer is almost always constrained by upwind distances from surface edges, i.e. fetch, and atmospheric stability (Foken, 2008a). In fetch limited conditions (small fields or plots), an 'ideal' surface layer (in the sense of MOST assumptions) rarely exists or is simply too shallow to accommodate the vertical distances needed for accurate gradient measurements for the utility of BREB or aerodynamic methods (Thom et al., 1975). Corrections for deployment of the aerodynamic method within the roughness sublayer (i.e. below the surface layer) were proposed (Cellier and Brunet, 1992; Mölder et al., 1999); however, they have never become routine — partly because they lack the universal form of their surface layer counterpart (i.e., they vary with leaf area density, adjustment length scale, thermal stratification, mean canopy height, etc.). Another reason is that EC measurements proliferated in the late 1990s within the research community, resulting in some disinterest in the aerodynamic method (Aubinet et al., 1999). Although BREB can technically operate in the roughness sublayer with no need for corrections (Cellier and Brunet, 1992), its validity still requires that mean gradient-diffusion theories (or K-theory) hold for describing turbulent fluxes and that the eddy diffusivity for heat and water vapor remain identical across all atmospheric stability conditions. The second requirement rarely holds in the roughness sublayer and there are numerous instances where K-theory entirely fails to describe turbulent fluxes (Cava et al., 2006; Kaimal and Finnigan, 1994; Raupach and Thom, 1981). Free of these mean 'gradient measurement' constraints but based on other assumptions, two popular and inexpensive methods have been proposed: the FV method (Tillman, 1972) and the SR analysis (Paw U and Brunet, 1991; Paw U et al., 1995). Their comparisons and possible modifications across various atmospheric stability regimes and vegetation cover frame the scope of this work.

The application of the FV method is relatively straightforward and only minor differences have been made after its original introduction. The FV method relies on the classical MOST relation between scalar standard deviation and an associated scalar flux scale. In the original study by Tillman (1972), H and friction velocity (u_*, m s^{-1}) under unstable conditions were estimated solely from the temperature variance measurement. The basic premise was that the dimensionless stability parameter $\xi = (z - d_o)/L_O$ needed in FV was empirically approximated from temperature high-passed time-series skewness (S_T), with z (m) being the measurement height, d_o (m) being the zero-plane displacement and L_O (m) being the Obukhov (1946) length. Subsequent studies typically used additional wind speed measurements combined with iterative procedure to obtain u_*, L_O and H simultaneously for all types of stratification (De Bruin et al., 1993; Paw U et al., 1995; Weaver, 1990). An important feature is that for $\xi \to -\infty$, i.e. free convection limit, FV becomes independent of u_* (De Bruin et al., 1993). Moreover, this free convection limit version of FV can be successfully applied across a wide range of unstable stability conditions, and thus has practical consequences allowing estimates of H from temperature measurements only (Albertson et al., 1995). Although FV relies on MOST or extended versions such as directional-dimensional analysis (Kader and Yaglom, 1990) and is thus strictly valid in the surface layer, it was demonstrated that the free convection limit of the FV provides reasonable estimates of H and LE under unstable conditions within the roughness sublayer (i.e., in a more dynamic region where MOST does not necessarily apply) provided the similarity constants are adjusted (Katul et al., 1995, 1996). This fact underscores the robustness of the FV scaling relations (Katul et al., 1996) – meaning that increases in scalar fluxes do translate to increases in scalar variances despite the anticipated surface heterogeneity in sources and sinks (absorbed by similarity constants).

Returning to the application of FV, the standard averaging duration in micrometeorology is 30 min providing a tradeoff between stationarity and statistical convergence of the time-averaging operator to ensemble averaging (Foken, 2008a). However, it is known that the variance during a given half-hour can dramatically increase due to low-frequency motion not associated with the surface turbulent flux (Dias et al., 2004). Therefore, different forms of high-pass filters are often employed in FV (De Bruin and Hartogensis, 2005; Tillman, 1972; Waterman et al., 2022). The cutoff frequency (f_c) value that delineates turbulence from other low-frequency modulations in temperature is somewhat ad hoc and often site or setup specific. The development of an objective method to determine the optimum f_c or the averaging period would be beneficial to standardize the use of the FV method for operational purposes.

In contrast to FV, numerous arguments and data processing approaches have been developed to determine H using SR. The SR analysis is based on the assumption that most of the turbulent flux is carried by intermittent, ramp-like, coherent (well correlated in time) structures. Determining the mean duration and mean amplitude of these coherent structures is therefore a crucial step in the SR analysis. In this context, the SR analysis had undergone several refinements since the pioneering study by Paw U and Brunet (1991) including application of digital bandpass filtering (Paw U et al., 1995), continuous and orthonormal wavelet analysis (Chen et al., 1997a; Katul et al., 1996) or application of higher-order structure functions to resolve mean characteristics of different pre-described ramp models assumed to be periodically repeating within the averaging period associated with the determination of the structure function (Chen et al., 1997a,b; Snyder et al., 1996; Spano et al., 1997). Besides the assumption about what portion of the flux is transported by coherent structures (Barthlott et al., 2007; Gao et al., 1989), the major uncertainty in the SR method is that the air volume associated with the coherent structure is not *a priori* known. For this and other reasons to be elaborated upon here, SR was presumed to require 'calibration' against independent methods, preferably EC (Drexler et al., 2004; Paw U et al., 1995). The original so called "alpha calibration" necessary for operational use of SR was partly overcome when SR was combined with K-theory and MOST (Castellví, 2004; Castellví et al., 2012, 2008). Several other variations of this combined method requiring additionally either mean temperature gradient measurements (Castellví, 2013), mean surface temperature (Castellví et al., 2016), or relying on knowledge of the production to dissipation rate ratio of turbulent kinetic energy (TKE) were further proposed (Castellví and Snyder, 2009) in attempts to reduce the ad hoc nature of the "alpha calibration". More recently, a different approach was suggested (Shapland et al., 2012a) for calibration with some success also reported (Shapland et al., 2012b, 2014; Suvočarev et al., 2014). This alternative is based on the premise that there exist coherent structures along two well-separated scales. The first scale (or scale I) occurs at higher frequencies and is typically not associated with flux-bearing eddies. At such high frequency, turbulence is presumed to be approaching a locally isotropic state and thus vertical velocity fluctuations are not correlated with temperature fluctuations (Pope, 2000). To identify the flux-bearing scale (or scale II), scale I ramp characteristics need to be determined first (Shapland et al., 2012b). Because the scale I structures can occur at very high frequencies when measurements are carried close to the surface, a sensor with a sufficiently fast response time is required. Alternatively, slower response sensors may be used subject to a sensor-specific correction (Shapland et al., 2014). Once the ramp characteristics of the scale II are determined, no further calibration is required in principle (Shapland et al., 2012b). It is noteworthy that the approaches proposed by Castellví (2004) and Shapland et al. (2012a) provide different perspectives on the signature of coherent structures and their flux-bearing contribution. The link between these two approaches requires further inquiry, which is to be partly addressed in this work. The SR methodology has been and remains under intensive development, thereby posing multiple challenges to standardization required for routine flux estimation over arbitrary agricultural or forest land cover. The goal here is to analyze the major SR formulations, compare them with EC and FV and provide further recommendation concerning the routine use

of SR and FV application. This comparison and critical appraisal is timely given the increasing popularity of SR method, recent commercialization of SR systems (e.g. https://tule.ag/) and their deployment in various environments including forests (Paw U et al., 1995; Zeri et al., 2013), wetlands (Drexler et al., 2004), crop fields (French et al., 2012; Shapland et al., 2012b; Snyder et al., 2006), orchards (Paw U et al., 1995; Suvočarev et al., 2014), vineyards (Shapland et al., 2012c; Spano et al., 2000), agroforestry systems (Holwerda et al., 2021) or even protected environments such as screenhouses (Mekhmandarov et al., 2015). Likewise, FV method has been deployed across various experiments (Wesely, 1988; Lloyd et al., 1991; Kustas et al., 1994; Albertson et al., 1995; Hsieh et al., 2008; French et al., 2012) including aircraft measurements (Kotani and Sugita, 2007) and even a unique study of the boundary layer of Mars (Davy et al., 2010). Due to its robustness and simplicity, FV has also been proposed as a gap-filling tool to EC measurements of multiple scalars when flux estimates are required almost continuously for water and carbon budgets (Guo et al., 2009) — again inviting their critical appraisal across different land cover and stability regimes. FV scaling is also routinely used in the land (and marine) surface models to link land–surface fluxes to turbulence statistics as done in the Cloud Layers Unified By Binormals (CLUBB) scheme (Waterman et al., 2022). As such, an assessment of FV across differing sites will benefit future revisions to these schemes.

From a broader perspective, a comparison between FV and SR may be a logical step to unpack connections between coherent structures (i.e. ramps) and the emergence of universal stability correction functions in temperature variances. To what degree do ramps contribute to heat exchange by virtue of them carrying much of the temperature variance? FV does not consider ramp characteristics in its inference of H and assumes that distance from d_0 is the appropriate length scale to describe temperature variance. Conversely, SR is based on detecting ramps whose characteristic length and time scales do not follow MOST. A bridge between FV and SR can begin informing why MOST scaling holds even when individual ramp characteristics rarely obey length and time scales associated with MOST.

2. Theory

In the analysis that follows, it is assumed that the flow above a canopy is stationary and planar homogeneous with no subsidence. Moreover, molecular diffusion of heat is ignored relative to the turbulent transport of heat. Under those conditions, the turbulent heat flux above the canopy can be assumed constant independent of distance from the ground or d_0. Unless otherwise specified, the following notation is used: t is time; $x = x_1$, $y = x_2$, and $z = x_3$ represent the longitudinal (aligned in the direction of the mean flow), transverse, and vertical (or wall normal) directions in a Cartesian coordinate system; $u = u_1$, $v = u_2$, and $w = u_3$ are the instantaneous velocity components (all in m s^{-1}) corresponding to directions x_i with $i = 1, 2, 3$, respectively; T (K) is the instantaneous air temperature; overlined quantities indicate ensemble-averaged components commonly determined from temporal averaging over 30 min, and primed quantities indicate fluctuating components determined by subtracting the average value from the instantaneous values.

The turbulent sensible heat flux H (W m^{-2}) is given as (Foken, 2008a; Stull, 1988)

$$H = \rho c_p \overline{w'T'}\,, \tag{1}$$

where ρ (kg m^{-3}) is the mean air density (overline dropped for notational simplicity), c_p (J kg^{-1} K^{-1}) is the specific heat capacity of dry air at constant pressure, $\overline{w'T'}$ (K m s^{-1}) is the kinematic sensible heat flux defined by the covariance between w' and T'. Likewise, air flow introduces a turbulent stress at the canopy top that is given by ρu_*^2, where $u_* = \sqrt{-\overline{u'w'}}$.

A distinction is made between the atmospheric surface layer (ASL) and the roughness sublayer (RSL) above canopies. In the ASL, which as earlier noted is some 2–3 h from the ground for scalars (Raupach and Thom, 1981), the 'effective' flux transporting eddies are assumed to be attached to the surface (or d_o) whereas in the RSL, they are influenced by canopy properties such as the canopy height h and may not scale with z.

2.1. The flux-variance method

In MOST, a non-dimensional temperature scale T_* (K) is introduced and defined as

$$T_* = -\frac{\overline{w'T'}}{u_*} = -\frac{H}{\rho c_p u_*}\,. \tag{2}$$

The characteristic length scale proposed by Obukhov (1946) relating mechanical generation and buoyancy production (or destruction) of TKE, i.e. L_O, is given as

$$L_O = -\frac{u_*^3}{\kappa \frac{g}{T}\frac{H}{\rho c_p}}\,, \tag{3}$$

where κ (= 0.4) is von Kármán constant and g (= 9.81 m s^{-1}) is the gravitational acceleration. This definition of L_O ignores the latent heat flux contribution, which is usually small. The L_O may be interpreted as the height from d_0 at which the mechanical production of TKE is balanced by buoyant production (or destruction for stable stratification) whereas d_0 is conventionally approximated or modeled from the centroid of the drag force acted upon by the vegetation on the air flow within the canopy volume (Jackson, 1981; Poggi et al., 2004). From Eq. (2), $u_* = -H/(\rho c_p T_*)$ and combining with Eq. (3) yields

$$H = \rho c_p \sqrt{\frac{\kappa g}{T} T_*^3 L_O}\,. \tag{4}$$

The sign of H cannot be predicted from Eq. (4) as T_* and L_O have the same sign. According to MOST, the temperature variance, σ_T^2 can be related to T_* and a non-dimensional stability parameter ξ through 'universal' functions expressing dimensionless temperature standard deviation (also known as integral turbulence characteristic or flux–variance similarity relation) as

$$\phi_T = \frac{\sigma_T}{|T_*|}\,. \tag{5}$$

Eq. (4) can now be rewritten as a FV method

$$H = \rho c_p \left(\frac{\kappa g (z - d_0)}{T}\right)^{1/2} \left(\frac{\sigma_T}{|\xi|^{1/3}\phi_T}\right)^{3/2}\,. \tag{6}$$

There are several parameterizations for ϕ_T (Foken, 2008a; Sfyri et al., 2018; Kaimal and Finnigan, 1994; Sorbjan, 1989; Tillman, 1972) but this function must approach a constant value when $|\xi| \to 0$. For $\xi \leqslant 0$, a widely used interpolation function satisfying these limits has the following form

$$\phi_T = C_1 \left(C_2 - \xi\right)^{-1/3}\,, \tag{7}$$

where C_1 and C_2 are similarity constants. For $\xi > 0$, different expressions exist including $\phi_T = C_3$ or $\phi_T \propto \xi^{-1}$ (Kaimal and Finnigan, 1994). Following Tillman (1972), $C_1 = 0.99$ (after adjustment of the originally used $\kappa = 0.35$ to the widely accepted value of 0.4), $C_2 = (C_1/C_3)^3$, and $C_3 = 1.77 - 2.5$. Under neutral conditions, $|\xi|$ approaches zero and ϕ_T converges to a constant value, C_3, while for the limiting case of free convection $-\xi \gg C_2$ and $\phi_T \approx C_1(-\xi)^{-1/3}$ (Albertson et al., 1995; Katul et al., 1996; Tillman, 1972). Hence, Eq. (6) for free convective conditions reduces to a u_* independent form (Tillman, 1972)

$$H = \rho c_p \left(\frac{\sigma_T}{C_1}\right)^{3/2} \left(\frac{\kappa g (z - d_0)}{T}\right)^{1/2}\,. \tag{8}$$

The robustness of this expression may also be inferred from Eq. (6). The term $|\xi|^{1/3}\phi_T$ rapidly approaches C_1 when $|\xi|/C_2 \gg 1$. With C_2 usually being a small constant, mildly unstable conditions ($|\xi| > 0.2$) satisfy

$[|\xi|/(C_2+|\xi|)]^{1/3} \rightarrow 1$ due to the sub-unity exponent (= 1/3). Even for $C_2 = 0.1$ and $|\xi| = 0.2$, $[|\xi|/(C_2+|\xi|)]^{1/3} = 0.87$, which is sufficiently close to unity for the purposes here.

Returning to stable atmospheric stability conditions ($\xi > 0$) and assuming $\phi_T = C_3$ (Tillman, 1972), Eq. (6) can be rearranged into

$$H = \rho c_p \frac{\sigma_T}{C_3} u_* , \tag{9}$$

indicating a linear dependence on u_* under stable stratification. A number of studies have shown that the free convection scaling (Eq. (8)) yields surprisingly reasonable predictions of H from measured σ_T even when the stability conditions are only mildly unstable, a result that popularized the use of the FV method (Albertson et al., 1995; Guo et al., 2009). Tillman (1972) also noted the non-Gaussian character of the air temperature time series (associated with the presence of ramp-cliff structures) and suggested that S_T or other higher odd moments can be used as an approximation of $-\xi \geqslant 0$. This approximation can lead to an empirical expression of Eq. (6) for the entire range of unstable conditions requiring only σ_T and S_T measurements. An interesting aspect of such formulation is that it allows an estimate of u_* and du/dz without requiring any velocity measurements.

2.2. The surface renewal method

The SR concept was originally introduced in chemical engineering by Higbie (1935) to predict the inter-facial heat transfer between the liquid and gaseous phases. In this concept, small parcels present at the interface are responsible for an unsteady diffusion transport of heat between two phases. The parcels remain at the interface for a certain amount of time (contact or residence time) and then are randomly replaced (renewed) by other parcels from the well-mixed turbulent layers located further away from the interface. It is assumed that this parcel renewal process is responsible for most of the heat transport between two phases. Higbie (1935) assumed uniform distribution for contact durations to predict a mean residence time. This assumption was refined and extended in many studies, for instance by accounting for random parcel motion and thus varying contact times beyond uniform (for more details see Katul et al., 1996). The connection between SR and ramp-like structures was first introduced by Paw U and Brunet (1991) and Paw U et al. (1995) to describe the exchange of heat and scalars at the canopy–atmosphere interface. This work marked a major departure from conventional SR theory because it presumes large eddies (or ramps), not Kolmogorov sized micro-eddies (Brutsaert, 1965; Katul and Liu, 2017), contribute to H. Thus, the SR schemes to be evaluated here are suggested as a logical corollary to findings that the turbulent transport of scalars is far from being random and is characterized by organized, intermittent coherent structures exhibiting ramp-like signatures (Gao et al., 1989; Paw U et al., 1992; Priestley, 1959; Tillman, 1972; Van Atta, 1977). Immediately above canopies, the existence of this high level of organization is perceived to be a consequence of Kelvin–Helmholtz like instability forming at the interface of two co-flowing fluids with different velocities as first proposed by Raupach et al. (1996) and further discussed elsewhere (Brunet and Irvine, 2000; Katul et al., 1998a; Thomas and Foken, 2006). The length scale of these coherent eddies is proportional to the mixing layer shearing scale associated with the inflection point of the mean longitudinal velocity profile (Brunet and Irvine, 2000; Foken, 2008a; Katul et al., 1998a; Raupach et al., 1996). These developments about the topological structure of coherent eddies immediately above dense canopies suggested that the frequency of coherent structures is related to wind shear (Barthlott et al., 2007; Katul et al., 1998a; Paw U et al., 1992; Shapland et al., 2012b) and not to buoyancy as previously conjectured by Priestley (1959). In fact, ramp-cliff patterns in high-frequency scalar concentration time series have been observed under near-neutral stratification (Paw U et al., 1992) and in laboratory studies (Warhaft, 2000). How to utilize the occurrence of such coherent structures in predicting mass and heat fluxes is what SR analysis seeks to answer (Paw U et al., 1992; Qiu et al., 1995). In the SR paradigm, most of the transport is assumed to be associated with such coherent structures (Paw U et al., 1995). It is to be noted that different studies reported significantly different relative contribution of coherent structures to scalar fluxes ranging from 0.4 to almost unity (Barthlott et al., 2007; Collineau and Brunet, 1993b). However, the identification of the aforementioned coherent structures also differed across those studies. Such differences complicate any generalization without further exploring how to standardize the definition and detection of coherent structures — at least for the purposes of SR analysis.

For simplicity, we restrict the explanation of the SR theory to the exchange of heat during unstable conditions (i.e. the canopy is warmer than the adjacent air) because these conditions are of interest to many agricultural and forestry systems. Also, the Reynolds number is likely to be sufficiently large under such unstable conditions ensuring that turbulence is fully-developed and an extensive inertial subrange at small scales may be reasonably delineated. Last, high Reynolds numbers are required to ensure ensemble Eulerian and Lagrangian flow statistics converge, an assumption that is implicit in all SR analyzes (conceptually formulated in the Lagrangian framework but implemented using Eulerian temperature statistics). During such conditions, it may be argued that a parcel of air originating from the reasonably well-mixed atmosphere above the canopy instantaneously penetrates into the canopy and begins to be heated by canopy elements. If we follow the parcel (Lagrangian perspective) and monitor its mean temperature, we would register steady temperature during the presence of the parcel above the canopy (assuming no significant heat diffuses by molecular motion), followed by gradual temperature increase during the period when the parcel is residing within the canopy. This stage would be followed by a temperature decrease as soon as the parcel ejects from the canopy. This entire process terminates by steady temperature roughly identical to the original one after the parcel becomes part of the bulk atmosphere above the canopy (Paw U and Brunet, 1991). The ensemble average of the parcels' temperature amplitudes would be then proportional to mean temperature gradient between the canopy and the atmosphere (Castellví, 2004; Castellví et al., 2002) and the rate of parcels' renewal to the vertical exchange velocity (Chen et al., 1997b). In practice, such Lagrangian parcel monitoring is difficult to carry out and Eulerian approaches must be used instead. In such a frame of reference, an expected air temperature pattern at the canopy top (i.e. the interface) would still be characterized by fluctuation between two boundary conditions, i.e. warmer surface and colder bulk atmosphere. The patterns would be, however, characterized by steep changes as the parcels passing along the sensors will differ in their elapsed contact time and thus will differ in their amount of heat received from the surface. The steepest change pertains to a gradually warmed parcel just replaced by a parcel form aloft leading to a sharp ramp-cliff pattern. In Eulerian monitoring, the depth of the cliffs in the ramp-cliff pattern would also be proportional to the mean temperature gradient between the canopy and the atmosphere, but ramps of all sizes will be 'infected' differently by advective processes that need to be judiciously filtered out, which is one of the main challenges to SR analysis (Paw U et al., 1995). To illustrate, if the air parcel is defined by a volume V, then its temperature changes over time (dT/dt) can be shown to be directly related to H (assuming, once again, loss of heat by molecular diffusion is small from the parcel after contact with the canopy) by

$$H = \rho c_p \frac{dT}{dt}\left(\frac{V}{A}\right) , \tag{10}$$

where V/A represents the ratio of the parcel volume to projected area (Paw U et al., 1995). This ratio converts the heating rate per unit of parcel volume (W m^{-3}) into a sensible heat flux density (W m^{-2}) expressed per area of the ground. It has to be stressed that Eq. (10) represents the Lagrangian perspective assuming that the total derivative of temperature with respect to time is known (Paw U et al., 1995).

A fixed temperature sensor (i.e., Eulerian) can only measure $\partial T/\partial t$ of a collection of parcels. The relation between the total and partial derivatives is

$$\frac{dT}{dt} = \frac{\partial T}{\partial t} + \frac{\partial u_j T}{\partial x_j}. \tag{11}$$

It is evident that Lagrangian renewal process is not possible to be described in a Eulerian sense without the three-dimensional velocity components. However, it can be shown that dT/dt may be approximated in several ways from Eulerian measurements of $\partial T/\partial t$ by applying several assumptions and filtering schemes. At the outset, the working assumption is that interactions between instantaneous velocity and spatial temperature gradients occur at higher frequencies compared to $\partial T/\partial t$. This time scale separation may enable the estimation of dT/dt from $\partial T/\partial t$. The five key assumptions and implementation tactics of such filtering are now reviewed.

(1) The first approach was proposed by Paw U and Brunet (1991) and simply assumes that $dT/dt = m\partial T/\partial t + b$ where m is the slope and b is an intercept. By computing the local time derivative $(T_t - T_{t-dt})/dt$ and considering only positive or negative local differences for unstable and stable conditions, respectively, the flux can be obtained by applying Eq. (10) adjusted by linear regression with independent measurement (e.g. EC).

(2) Alternatively, the advective parts in the Eq. (11) can be eliminated by band-pass sine filtering, where the center frequency between two f_c represents the average ramp occurrence and must be estimated *a priori*. For this purpose, an empirical scaling with shear was proposed and used (Paw U et al., 1995). Although it brings the requirement for additional wind speed measurements, it was suggested that an average site wind speed can be used for this purpose (Paw U et al., 1995). The flux is then calculated by applying the above-mentioned local finite differencing.

(3) The third approach is an alternative to the second one where the isotropic high-frequency advective terms are eliminated using the orthonormal wavelet transform in conjunction with a universal wavelet thresholding technique (Katul et al., 1996). This approach assumes that interaction between velocity and air temperature fluctuations occurs at higher frequencies, thereby rendering a scale separation between $\partial T/\partial t$ and the advective terms. The filtering assumes that the high frequency is associated with small wavelet amplitudes (resembling random motion) while the low frequency is assumed to be associated with a small number of energetic wavelet coefficients to be retained. Because the filtering is conducted in the wavelet domain, the sharp structures at the end of the ramps are not smoothed by this filtering approach, which is unavoidable using a bandpass filtering in the Fourier domain with poor locality in time. In this orthonormal wavelet filtering scheme, only the high-frequency component is removed whilst the low-frequency motion, associated with coherent structures, but also possibly with other non-turbulent structures, are preserved. For proper flux determination, the removal of the low-frequency part would be also necessary, especially at sites with frequent non-stationarity (Zeri et al., 2013). Since the orthonormal wavelet transform has limited frequency resolution, especially in the low-frequency end of the spectrum, a Fourier transform with bandpass or high-pass filtering capacity can be applied for the removal of low-frequency motion as proposed in some studies (Katul et al., 1996).

(4) The fourth approach is based on prior research linking the effects of coherent motion on structure functions (Van Atta, 1977, 1978). The structure function is defined as the mean value of the time difference of the temperature raised to some exponent. In discrete form, the nth-order structure function is

$$\overline{S^n(r)} = \frac{1}{N-j}\sum_{i=1+j}^{N}(T_i - T_{i-j})^n, \tag{12}$$

where $\overline{S^n(r)}$ is the structure function for a statistical moment n, r is the time (or space) lag between the differenced points, j is the sample lag between the different points related to r by $j = rf$ where f is the sampling frequency (Hz), and N is the number of points in the time series. Van Atta (1977) hypothesized that the temperature time series can be decomposed into repeated random and coherent (dominated by a ramp-cliff pattern) parts that are statistically independent. With this assumption, their second ($n = 2$), third ($n = 3$) and fifth ($n = 5$) order structure functions can be computed as

$$\overline{S^2(r)} = \overline{S^2(r)_{coherent}} + \overline{S^2(r)_{random}}, \tag{13}$$

$$\overline{S^3(r)} = \overline{S^3(r)_{coherent}}, \tag{14}$$

$$\overline{S^5(r)} = 10\overline{S^2(r)_{random}}\ \overline{S^3(r)_{coherent}} + \overline{S^5(r)_{coherent}}. \tag{15}$$

It is to be noted that for $n = 3$, only the coherent part contributes to $\overline{S^3(r)}$ as the random component cancels out assuming that the random noise has a symmetric probability density function. To estimate the individual ramp and turbulence contributions to the measured structure function, Van Atta (1977) proposed a model for the joint distribution of the ramp amplitude (a), the length composed of the quiescent period (s) and the gradual rise period (d) and the repetition rate (SI 1). The moments of this distribution for the same three orders are

$$\overline{S^2(r)} = \frac{a^2 r}{d+s}\left[1 - \frac{1}{3}\left(\frac{r}{d}\right)^2\right], \tag{16}$$

$$\overline{S^3(r)} = \frac{a^3 r}{d+s}\left[-1 + \frac{3}{2}\frac{r}{d} - \frac{1}{2}\left(\frac{r}{d}\right)^3\right], \tag{17}$$

$$\overline{S^5(r)} = \frac{a^5 r}{d+s}\left[-1 + \frac{5}{2}\frac{r}{d} - \frac{10}{3}\left(\frac{r}{d}\right)^2 + \frac{5}{2}\left(\frac{r}{d}\right)^3 - \frac{2}{3}\left(\frac{r}{d}\right)^5\right]. \tag{18}$$

Chen et al. (1997a) noted that ramps have typically non-instantaneous termination and proposed an alternative ramp model with a finite microfront time, but no quiescent period, which described the measured structure functions better than the model originally proposed by Van Atta (1977). In this approach, three parameters describing the ramp properties can be either fitted, which then typically requires measurement at higher frequencies than 10 Hz. Alternatively, d can be derived independently by applying a continuous wavelet ramp detection method (Chen et al., 1997a; Collineau and Brunet, 1993a), or d can be obtained from an empirical relation with u_* (Chen et al., 1997b; Raupach, 1989).

For r much smaller than d and s, Eqs. (16)–(18) can be simplified as $\overline{S^n(r)} = (-a)^n\, r/(d+s)$ and their combination further yields a cubic equation for the ramp amplitude

$$a^3 + a\left[10\overline{S^2(r)} - \frac{\overline{S^5(r)}}{\overline{S^3(r)}}\right] + \overline{S^3(r)} = 0, \tag{19}$$

which can then be solved for its real roots. By inserting the obtained amplitude into the rewritten form of the cubic structure function, the sum of the gradual rise and quiescent period can be solved as

$$d + s = \frac{-a^3 r}{\overline{S^3(r)}}. \tag{20}$$

Eqs. (19) and (20) are hereafter referred to as the Van Atta (1977) solution abbreviated as "VA". Eqs. (16)–(20) can be solved in their complete form if d is determined by applying the simultaneous solution of $\overline{S^3(r)}/\overline{S^3(br)}$ where b is an integer ensuring $br < d$ and $br < s$ (Paw U et al., 2005). Assuming that dT/dt from Eq. (10) is equal to a/d and by multiplying this expression by the relative time for heating $d/(d+s)$, a new form of Eq. (20) can be obtained (Snyder et al., 1996) and is given by

$$H = \rho c_p \frac{a}{d+s}\left(\frac{V}{A}\right). \tag{21}$$

Apart from $r \ll d$ and $r \ll s$, it is not explicit which time lag r should be used for applying the VA solution. Some authors opted to use a set of r and after selecting the one providing best agreement with EC measurements (French et al., 2012; Rosa et al., 2013; Rosa and

Tanny, 2015; Snyder et al., 1996). Others used the average H obtained from several r (Shapland et al., 2012c; Spano et al., 1997, 2000). More universal approach proposed by Chen et al. (1997a) was to select an r that resulted in the first global maximum of the cubic structure function normalized by r (Castellvi, 2007; Castellví, 2004; Castellví and Snyder, 2010; Castellví et al., 2008, 2006; Shapland et al., 2012a,b, 2014, 2012c; Suvočarev et al., 2014). It should be clarified that the varying of H with r is partly an artefact of the linearization invoked in Eqs. (16)–(18) rather than evidence that specific r is related to an effective eddy size $\sim \alpha z$ (see the next section). This can be demonstrated by applying the complete VA solution that provides consistent H and hence αz for a larger range of r. According to Shapland et al. (2012a), the flux-bearing scale II can be resolved using larger r for which they argued that $\alpha \sim 1$. Therefore, the dependence of mean eddy sizes on r is possible but perhaps obscured by errors emerging due to linearization in the VA solution.

(5) Although it has not been directly applied as a tool to obtain fluxes using SR, an approach based on coherent structures detection using a continuous wavelet transform (Collineau and Brunet, 1993a,b; Thomas and Foken, 2006; Barthlott et al., 2007) is also considered here. The ramp duration is first determined using a continuous wavelet transform employing the second derivative of a Gaussian function (also called "Mexican Hat") as the analyzing wavelet. The Mexican Hat is a symmetric wavelet ensuring no asymmetries in the wavelet coefficients arise from the transformation itself. In this approach, the scale associated with the highest energy (or the peak of the continuous wavelet power spectrum) is characterized by an unambiguous zero crossing at each end of the ramp. After the ramp duration is determined, a linear regression can be applied to estimate the slope of each individual ramp that can then be used to determine the mean ramp amplitude.

2.3. The size of air parcel relevant in SR

Apart from the correct detection of coherent structures from time series containing additional advective terms, the volume of the air parcel associated with the coherent structure has to be inferred. That is, in the right-hand side of Eqs. (10) and (21), V/A has to be estimated. In early studies within RSL (Katul et al., 1996; Paw U et al., 1995) it was assumed that V/A is proportional to canopy height h. In an attempt to estimate the proportionality constant, it was later assumed that the parcels are not heated homogeneously with depth within the canopy volume and roughly one half of the air parcel (assuming linear decrease of heating with height) was considered to be related to dT/dt. Eq. (10) can then be rewritten as

$$H = \alpha h \rho c_p \frac{dT}{dt}, \tag{22}$$

where α is a newly introduced empirical parameter set to 0.5 in studies by Paw U et al. (1995) and Katul et al. (1996). In other studies over short canopies (Snyder et al., 1996; Spano et al., 1997, 2000), it was assumed that V/A scales with z. This led to a modification of Eq. (10) into

$$H = \alpha z \rho c_p \frac{dT}{dt}, \tag{23}$$

where α becomes height dependent (Paw U et al., 2005). In general, it was found that α is close to unity when measurements are conducted in the ASL assuming quasi-homogeneous heating of the parcel that scaled with z and that $\alpha \sim 0.5$ better describes the SR calculations when measurements are conducted close to the top of dense canopies in the RSL. Although it can be perceived that the volume of air parcel in the study by Paw U et al. (1995) and Katul et al. (1996) scaled with h because the sensors were deployed near the canopy top and so Eqs. (22) and (23) are equivalent, the logic behind them may be explained by the fact that mean eddy sizes transporting momentum in RSL scale with h, whereas in ASL, they scale with $z - d_0$ (Poggi et al., 2004; Raupach et al., 1996). Further investigations indicated that α also depends on the thermocouple size or, more generally, on the sensor frequency response (Duce et al., 1998; Shapland et al., 2014). In this sense, the parameter α can be perceived as an integrative empirical parameter that must be determined for a specific surface cover and measurement height as well as the frequency response of the sensors deployed. Since surface conditions often vary over time, several calibrations with independent methods would be necessary (Rosa and Tanny, 2015). Castellví et al. (2002) and Castellví (2004) already pointed out this lack of generality in the SR method and provided an independent solution explaining the variation of α based on a combination of SR analysis and a one-dimensional diffusion equation. During the daytime conditions in the mixed layer, H varies in the vertical across the entire atmospheric boundary layer. In this case, the vertical transfer of heat can be described using a one-dimensional diffusion equation (Berkowicz and Prahm, 1979; Priestley, 1959; Stull, 1988)

$$\frac{\partial T_{(t,z)}}{\partial t} = -\frac{\partial}{\partial z}\overline{w'T'} = \frac{\partial}{\partial z}\left(K_h \frac{\partial T_{(t,z)}}{\partial z}\right), \tag{24}$$

where K_h (m s^{-1}) is the turbulent transfer coefficient or eddy diffusivity for heat. The solution of Eq. (24) can be facilitated using a fractional calculus method assuming K_h is a constant independent of z (Wang and Bras, 1998). By adopting this assumption, the vertical gradient of T can be expressed as a weighted average (half-order derivative) of the T time-series at a given z (Wang and Bras, 1998; Wesson et al., 2001), where the weights depend on $(ds')(t-s')^{-1/2}$, t is as before time and s' is an integration variable that varies from $s' = 0$ to $s' = t$. Taking the outcome of half-order time derivative and assuming that only the coherent part of turbulence is associated with the turbulent exchange, subsequent integration of the mean ramp-like structure over the mean $d+s$ (with a reasonable assumption that the microfront period is negligible as compared to $d + s$) results in following expression

$$\frac{\partial T_{(t,z)}}{\partial z} = -\frac{a}{\sqrt{\pi K_h (d+s)}}, \tag{25}$$

relating ramp amplitude with the vertical gradient between the net heat source and the bulk atmosphere from where the fresh air is sweeping toward the surface (Castellví, 2004). By setting $K_h = \kappa(z - d_0)\, u_*/\phi_h$ (Stull, 1988) and after combining with Eqs. (21), (23) and (25) yields (Castellví, 2004)

$$\frac{V}{A} = \alpha z = \sqrt{\frac{\kappa(z-d_0)}{\pi}(d+s)\frac{u_*}{\phi_h}}, \tag{26}$$

with

$$H = \rho c_p a \sqrt{\frac{\kappa(z-d_0)}{\pi(d+s)}\frac{u_*}{\phi_h}}, \tag{27}$$

where ϕ_h is a universal stability correction function for exchange of heat that varies with the dimensionless stability parameter ξ in the ASL. The term αz in Eq. (26) can be interpreted as the volume of air per unit ground area exchanged on average for each ramp (Castellví, 2004; Chen et al., 1997b) or effective eddy sizes of renewed air parcel with frequency $(d + s)^{-1}$ (Castellví, 2004). To apply the SR analysis in conjunction with Eq. (27), additional measurement of u_* and L_O or an iterative procedure to estimate u_* and L_O from additional u measurements (i.e., 2D or 3D anemometer) is required. Several other follow up versions have been proposed to eliminate the dependency on u_* yet requiring additionally either temperature gradient (Castellví, 2013) or surface temperature (Castellví et al., 2016) measurements. In this study, we further consider and evaluate only an expression derived from the combination of SR and the dissipation method (Hsieh et al., 1996) following (Castellví and Snyder, 2009; Gray et al., 2022)

$$H = \rho c_p \frac{a}{|a|}\frac{G_k}{\pi}(z-d_0)\frac{a^2}{\sigma_T(d+s)}, \tag{28}$$

since it does not require any additional instrumentation than the fast response thermocouple. The newly introduced parameter G_k in Eq. (28)

emerges from convergence of $\kappa\,\phi_T/\phi_h$ over wide range of unstable conditions (Hsieh et al., 1996).

Eqs. (24) and (25) are, in principle, applicable to averaging periods much longer than the ramp-duration time scale but much shorter than changes in meteorological conditions. The interpretation offered in Eq. (26) requires that Eqs. (24) and (25) be extended to turbulent time scales commensurate with ramps, which is questionable. However, it should be noted that the structure function analysis integrates over 30 min intervals and thus the resulting ramp characteristics do not represent single ramp events but ensemble (or time averaged) ramps.

2.4. A new perspective on SR

Formally, Eq. (24) describes flow that is not stationary and is not compatible with $K_h = \kappa(z-d_0)\,u_*/\phi_h$ (i.e. MOST). Also, much of $\overline{w'T'}$ in the mixed layer is not due to the diffusive part but due to the non-local part (Ghannam et al., 2017) exemplified by the eddy diffusivity-mass flux (or EDMF) approach. An entirely different perspective based on the original SR concept pioneered by Higbie (1935) is now offered. At the contact point between the surface and the bulk fluid, the air temperature is assumed to be transferred by molecular diffusion resulting in

$$\frac{H_{(t,0)}}{\rho c_p} = -D_m \frac{\partial T_{(t,0)}}{\partial z}\,;\; \frac{\partial T_{(t,z)}}{\partial t} = D_m \frac{\partial^2 T_{(t,z)}}{\partial z^2}\,, \tag{29}$$

where D_m is now the molecular diffusion coefficient. The boundary conditions for $\partial T_{(z,t)}/\partial t$ are represented by the temperature of the surface $T_{(t,z=0)} = T_s$ and by the temperature of the bulk atmosphere $T_{(t,z\to\infty)} = T_b$. Here, it is assumed that the source and sink of heat are constant, and hence T_s and T_b do not change with time due to the rapid exchange process. The instance when the surface is renewed with the bulk fluid, the initial condition in Eq. (29) satisfies the third condition $T_{(t=0,z)} = T_b$. By imposing these boundary conditions, the solution of Eq. (29) is given by (Sutton, 1953; Priestley, 1959; Crank, 1975)

$$T_{(t,z)} = (T_b - T_s)\; erf\left(\frac{z}{2\sqrt{D_m t}}\right) + T_s\,, \tag{30}$$

where $erf(.)$ is an error function or so-called Gauss error function defined as $erf(x) = 2\pi^{-1/2}\int_0^x e^{-t^2}$ (Crank, 1975). To obtain the heat flux at the surface, Eq. (30) is differentiated with respect to z and upon setting $z = 0$ yields

$$H_{(t,0)} = -\rho c_p D_m \frac{\partial T_{(t,0)}}{\partial z} = -\rho c_p D_m \frac{(T_b - T_s)}{\sqrt{\pi D_m \tau}}\,. \tag{31}$$

In Eq. (31), the contact duration τ is presumed to be a random variable and is associated with one renewal event. Hence, the overall H requires averaging over all contact durations between eddies impinging onto the surface over the usual time averaging period (30 min here). Likewise, $\sqrt{\pi D_m \tau}$ may be interpreted as the thickness of the sublayer arising from the molecular diffusion of heat into the air parcel in contact with the surface due to a single renewal event. In field conditions, $z = 0$ is no longer well defined because of the presence of roughness elements characterized by a momentum roughness height z_o. A fixed sensor at some height $z \gg z_o$ above the surface is also measuring wide ranging eddy sizes passing the sensor including those that are much smaller or larger than predicted by the mixing length theory (i.e. κz). In that case, considering one ramp event as a renewal event, $T_b - T_s$ can be replaced by the ramp amplitude a_i (the subscript i indicates an individual single ramp event), the contact time τ becomes $d_i + s_i$, and D_m must be replaced by an appropriate effective diffusion coefficient (D_e) reflecting the propagation of the diffusive heat front into the eddy at height z over $d_i + s_i$. In this case, the heat transported by a single ramp (or renewal event) making contact with the ground is

$$H_{(d+s,z)} = \rho c_p D_e \frac{a_i}{\sqrt{\pi(d_i + s_i)D_e}}\,, \tag{32}$$

where $\sqrt{\pi(d_i + s_i)D_e}$ is now measuring the effective diffusion depth of heat within an individual ramp detected at height z. This analysis presumes that the collision frequency of Kolmogorov sized eddies with the surface are not the main limiting factor (i.e. there is no shortage of Kolmogorov eddies that can be delivered to the surface and conduct heat exchange with the nearby atmosphere). The heat exchange process is thus presumed to be restricted by the ability of large-scale features needed to deliver the Kolmogorov eddies to the surfaces. Under this assumption, and to proceed from a single-ramp event to 30 min averaged heat fluxes, an ensemble averaging over all ramp occurrences at height z is required. Assuming ramps occur independently, then ensemble averaging over all ramps may be achieved with $\overline{a_i} = a$ and $\overline{d_i + s_i} = d + s$, where a, d, and s are inferred from structure function analysis, and $\overline{D_e} \approx K_h$ from MOST in Eq. (32). The ensemble-averaged Eq. (32) over all ramps is identical to Eq. (27) proposed by Castellví (2004) although based on a different set of assumptions. To illustrate, the time-averaged sensible heat flux (over 30 min) that is independent of z as required by MOST (but not by Eq. (24)), averaging Eq. (32) over all ramp events detected at height z leads to

$$-\rho c_p D_m \frac{\overline{\partial T_{(t,0)}}}{\partial z} = -\rho c_p D_m \frac{(T_b - T_s)}{\sqrt{\pi D_m}}\overline{\left(\frac{1}{\sqrt{\tau}}\right)} = \rho c_p K_h \frac{a}{\sqrt{\pi(d+s)K_h}}\,. \tag{33}$$

In the so-called micro-eddy model with exponentially distributed contact durations (Katul and Liu, 2017),

$$\overline{\left(\frac{1}{\sqrt{\tau}}\right)} = \left(\frac{\varepsilon}{\nu}\right)^{1/4}\,, \tag{34}$$

where ε is the mean TKE dissipation rate near the surface and ν is the kinematic viscosity of air. As such, with finite dissipation in the RSL now estimated from mechanical production of TKE in RSL influenced by z_o (i.e. $\varepsilon \sim u_*^3(\kappa z_o)^{-1}$), a link between the roughness Reynolds number ($Re_* = u_* z_o/\nu$), molecular Schmidt number ($Sc_m = 0.62$ for heat), and SR ramp characteristics can be established. After some algebra, it can be shown that

$$\frac{a}{T_s - T_b} = Sc_m^{-1/2} Re_*^{1/2}\left(\kappa \frac{u_*^2\,(d+s)}{K_h z}\right)^{1/2}\,. \tag{35}$$

For near-neutral conditions, $K_h = \kappa z\, u_*$ and

$$\frac{a}{T_s - T_b} = Sc_m^{-1/2} Re_*^{1/2}\left((d+s)\,\frac{u_*}{z}\right)^{1/2}\,, \tag{36}$$

where u_*/z is a characteristic shear time scale normalizing the mean ramp duration. The main result here is that the normalized mean ramp amplitude scales with two factors. The first is $Re_*^{1/2}$, which implies that rougher surfaces (such as forests) should have a larger normalized ramp size. The second is the normalized mean ramp durations, where reducing z and increasing u_* can also have a similar effect of amplifying the normalized ramp amplitude. In the case of periodic continuous renewals, the average ramp occurrence frequency and ramp durations must be related so that $d+s$ is linked to $1/f_c$, where f_c itself was shown to scale with u_*/z (or u_*/h) as discussed elsewhere (Paw U et al., 1995; Chen et al., 1997b). If so, then normalized mean ramp durations may play less of a crucial role in normalized mean ramp amplitudes when compared to $Re_*^{1/2}$.

Returning to the estimation of α, combining Eqs. (26) and (27) with Eq. (3) and expressing the outcome as dependencies on L_O and ϕ_h yields

$$\frac{V}{A} = \alpha z = \left(\frac{-a\; L_O \kappa^4\; g(z-d_0)^3\; (d+s)^2}{\pi^3\; T \phi_h^3}\right)^{1/5}\,, \tag{37}$$

and

$$H = \rho c_p \frac{a}{|a|}\left(\frac{a^6\; |L_O| \kappa^4\; g(z-d_0)^3}{\pi^3\; (d+s)^3\; T \phi_h^3}\right)^{1/5}\,. \tag{38}$$

As also pointed out by Castellví (2004), further analysis of $(|L_O|/\phi_h^3)^{1/5}$ suggests that H is insensitive to this quantity for a certain range of stability conditions. Therefore, fixing $(|L_O|/\phi_h^3)^{1/5}$ to a constant value for unstable and stable cases may be considered as one of the possible practical forms of the SR method independent of calibration.

Alternatively, by combining the expression for T_* (Eq. (2)) with the definition of L_O (Eq. (3)) and ϕ_T (Eq. (5)), it follows that

$$u_* = \sqrt{|L_O|\kappa g \frac{\sigma_T}{T\phi_T}}\,. \tag{39}$$

Inserting Eq. (39) into Eq. (26) and after some algebra yields

$$\frac{V}{A} = \alpha z = \kappa^{3/4}\sqrt{\frac{(z-d_0)\,(d+s)}{\pi}}\left(|L_O|\; g\frac{\sigma_T}{T}\right)^{1/4}\phi_h^{-1/2}\phi_T^{-1/4}\,, \tag{40}$$

and combining with Eq. (21) results in the following SR form

$$H = \rho c_p \kappa^{3/4}\; a\;\sqrt{\frac{(z-d_0)}{\pi(d+s)}}\left(|L_O|\; g\frac{\sigma_T}{T}\right)^{1/4}\phi_h^{-1/2}\phi_T^{-1/4}\,. \tag{41}$$

The advantage of Eqs. (38) and (41) is that if L_O can be sufficiently approximated from S_T or other statistics as originally suggested by Tillman (1972), the varying parameter α and H may be obtained without the need for velocity measurements as is required to solve Eq. (27). Eq. (26) combined with Eq. (21) and the VA solution was several times proven to be universally valid with no additional calibration (Castellví, 2004; Castellví et al., 2012; Castellví and Snyder, 2010; Suvočarev et al., 2014). What is unclear is why this solution is not sensitive to sensor frequency response as the method was shown to perform reasonably despite using different thermocouple sizes or sonic anemometers for air temperature measurements. More recent studies by Shapland et al. (2012a,b, 2014) hypothesized that there are coherent structures of multiple scales and that if a sensor with prefect frequency response is chosen, the VA solution is in most cases determining the coherent structures of the non-flux-bearing scale. Therefore, Shapland et al. (2012a,b) extended the VA solution for two-scale ramp time series where only the second scale is the flux-bearing and for that scale $\alpha \sim 1$ and the flux scales with z. Therefore, Eq. (23) can be applied in conjunction with what is termed as scale II ramp characteristics.

2.5. Combining FV and SR methods in the ASL

By combining Eq. (6) with Eq. (38) or Eq. (41), it becomes evident that matching H from FV and SR leads to only one unknown, i.e. L_O. Equating H from FV and SR and keeping the known variables on the right-hand side yields

$$\frac{\phi_h^2}{|\xi|\phi_T^5} = \frac{\kappa(z-d_0)}{\pi^2\; g(d+s)^2}\left(\frac{a}{\sigma_T}\right)^4\frac{T}{\sigma_T}\,. \tag{42}$$

The right-hand side of Eq. (42) shows how large-scale features associated with ramp statistics (a, d and s) explain their contributions to σ_T for different atmospheric stability conditions (ξ) at a pre-determined wall-normal distance $\kappa(z-d_o)$. Assuming MOST is valid, Eq. (42) also suggests that one can solve L_O only from the variables obtained from the high-frequency temperature measurements. As a consequence, H either from Eq. (6) or Eq. (38) and u_* from Eq. (39) can be computed. An explicit derivation of L_O from Eq. (42) is cumbersome and for many forms of the universal stability functions not feasible. Therefore, a numerical iterative procedure might be applied yet attention must be given to the choice of stability functions such that they satisfy only one and not multiple solutions. In an attempt to facilitate an explicit solution, the relation between ϕ_h and ϕ_T may be beneficial but even a simple expression between these two proposed by Foken et al. (1991) is not amenable to explicit solution of Eq. (42). More complex expressions relating ϕ_h and ϕ_T through second order closure schemes of temperature variance dissipation (Meyers and Paw U, 1986; Siqueira and Katul, 2002; Waterman et al., 2022) result in requirement for additional universal function for momentum and TKE. Hence, the expression provided in Eq. (42) cannot be further simplified in an analytical way. Nevertheless, one of the ways to simplify Eq. (42) is to empirically relate the quantity $\chi = \phi_h^2/(|\xi|\phi_T^5)$ with ξ. Since χ is the ratio of the universal functions and the stability parameter, it should scale with ξ in a universal manner that should be transferable from site to site. This assumption and its implications for deriving H only from temperature data will be tested here.

2.6. A modification for the RSL

All the preceding FV and SR formulations originating from MOST are valid in the ASL where the mixing length L_m scales with $(z-d_0)$. Because in the RSL the diffusivity and L_m remain nearly constant with z (Kaimal and Finnigan, 1994; Raupach and Thom, 1981), L_m throughout the RSL should be equivalent to L_m at the lowest level where MOST holds to ensure continuity. This level is assumed to be located at the top of RSL and hence is determined by RSL thickness (z^*, m) leading to a scaling of L_m with $\kappa(z^*-d_0)$ in the RSL (Cellier and Brunet, 1992; Raupach and Thom, 1981; Raupach et al., 1980). Consequently, whenever $z < z^*$, z^*-d_0 is used instead of $z-d_0$. As a consequence, FV and MOST based SR expressions are sensitive to the estimate of z^*. A synthesis of existing literature suggests $z^*/h = 2$–3 for tall and dense vegetation as discussed elsewhere (Brunet, 2020).

3. Materials and methods

The study was conducted at three research sites representing agricultural, forestry and agro-forestry systems during the years 2015 and 2016. In terms of measurement setup, the sites represent an ASL, a RSL, and a transitional layer. The overview of site characteristics and instrumentation are summarized in Table 1. A brief review of the individual sites is also offered for completeness.

3.1. Polkovice site (the Czech Republic)

The agricultural experimental field site is located in Polkovice (POL) within the Moravian part of the Czech Republic. The site is situated in a typical agricultural region known for its deep fertile soil and high productivity. The 26-ha field has a rectangular shape with a length of 800 m and a width of 325 m. The climate is temperate with a long-term (1981–2010) average daily air temperature of 9.3 °C and an average annual precipitation of 556 mm (Table 1). The soil type is luvic chernozem on the bedrock material loess, and during the growing season in 2015, it was covered with winter wheat (*Triticum aestivum*, variety Genius E). The observations used in the study were taken between early July till mid September 2015 (Table 1). The winter wheat was harvested on 5th of August 2015 followed by a period when the surface was characterized by a stubble, bare soil and lately emerging weeds. The maximum crop height was 1.0 m and after the harvest there was 0.1 m tall stubble. The plant area index (PAI) was measured by SS1 SunScan Canopy Analysis System by Delta-T Devices Ltd (Cambridge, United Kingdom). The area averaged PAI reached ~7.7 m^2 m^{-2} in early July and then slightly dropped to ~7.0 m^2 m^{-2} during the pre-harvest period. After the harvest, it was estimated to be ~0.3 m^2 m^{-2}. The instruments for micrometeorological measurements were deployed near the middle of the field aligned to the prevailing northwest wind direction. The field is flat and sufficiently large with sufficient fetch to be established (maximum and minimum are 555 m and 183 m, respectively). More details about the experimental site and instrumentation can be found elsewhere (Pozníková et al., 2018).

Table 1
Overview of the sites, vegetation cover, and the main EC, FV and SR instrumentation used for the three experimental sites.

Site	Polkovice (POL)	Alligator River (ALR)	Lenoir (LEN)
Country	the Czech Republic (CZ)	USA, North Carolina	USA, North Carolina
Longitude (°)	17.246	−75.904	−77.469
Latitude (°)	49.395	35.788	35.264
Elevation (m a.s.l.)	200	1	12
Mean annual temperature (°)	9.3	16.9	16.2
Mean annual precipitation (mm)	556	1270	1264
Site description reference	Pozníková et al. (2018)	Miao et al. (2017)	Tian et al. (2017)
Period of operation in this study	2015-07-02 to 2015-10-02	2016-03-20 to 2016-09-01	2015-06-03 to 2015-11-17
Surface cover and vegetation	wheat field/stubble and bare soil	forested wetland	pine-switchgrass intercrop
Plant area index (m^2 m^{-2})	0.3–7.7	0.9–5.5	4.0
Canopy height (m)	0.05–1.0	16.1–23.2	6.8–7.2
Zero plane-displacement (m)	0.03–0.8	11.0–19.0	5.5–5.8
Roughness layer depth (m)	0.15–1.7	28.8–55.67	12.5–13.2
Flux-variance and surface renewal			
Measurement height	3.4	32.9	7.1–7.5
Thermocouple type	CHCO-003	CHCO-003	CHCO-003
Thermocouple size (μm)	75	75	75
Sampling frequency (Hz)	10	10	10
Datalogging system	CR1000	CR1000	CR1000
Averaging period (min)	30	30	30
Eddy covariance			
Measurement height	2.7	33.2	7.1–7.5
Gas analyser	LI-7500A	LI-7200	–
Sonic anemometer	Gill Windmaster	Gill Windmaster/CSAT3	Gill Windmaster
Sampling frequency (Hz)	10	10	10
Datalogging system	LI-7550	LI-7550	LI-7550
Averaging period (min)	30	30	30
Software	EddyPro (version 6.0.0)	EddyPro (version 6.0.0)	EddyPro (version 6.0.0)

3.2. Alligator river site (North Carolina, USA)

The forest study site is located at the Alligator River National Wildlife Refuge (ALR), on the Albemarle–Pamlico peninsula of North Carolina, USA. The mean annual temperature and precipitation, from climate records of an adjacent meteorological station (Manteo, NC, National Climatic Data Center, 35.917°, −75.701°) for the period 1981–2010, were 16.9 °C and 1270 mm, respectively (Table 1). The forest type is a mixed hardwood swamp forest. The overstory is predominantly composed of black gum (*Nyssa sylvatica*), swamp tupelo (*Nyssa biflora*) and bald cypress (*Taxodium distichum*), with occasional red maple (*Acer rubrum*) and white cedar (*Chamaecyparis thyoides*). The understory is predominantly fetterbush (*Lyonic lucida*), bitter gallberry (*Ilex galbra*), and red bay (*Persea borbonia*). The major soil series are poorly drained Pungo and Belhaven mucks. The micrometeorological measurements were carried out at the 33 m tall scaffold tower within the forest with fetch extending more than 2.5 km in all directions. Due to the mixed species composition, a certain spatial variation in canopy height and PAI was expected. Both FV and SR require the d_0 and ignoring its spatial variation could lead to higher uncertainty in H estimates. The North Carolina Emergency Management Spatial Data Download QL2 LiDAR (2 points m^{-2}) together with a ten-foot grid raster digital elevation model were used to estimate the local height variations of the canopy from point cloud LiDAR and raster elevation data using an R package lidR (Roussel et al., 2020). An inverse distance weighting algorithm within 2.5 m search radius of classified canopy reflections > 0.5 m above the ground was used for interpolation (Chasmer et al., 2011). Further, to compute d_0, PAI was needed (Shaw and Pereira, 1982; Hall, 2002). This data were obtained from the 4-day Moderate Resolution Imaging Spectroradiometer leaf area index composite product MCD15A3H. To provide temporally continuous time series and to minimize the noise in the original data, a FlexFit (Gao et al., 2020) moving window filter approach using the polynomial fitting from nearby dates was used. Since the footprint of the micrometeorological measurement of fluxes is fluctuating in time, mean canopy height within the modeled footprint (Kljun et al., 2015) for each half-hour was computed. Moreover, because h, d_0 and hence PAI are affecting footprint in which these variables need to be determined, the computation needed to be solved iteratively. As a result of spatiotemporal variation of PAI and spatial variation of h and d_0, relatively wide range of these variables and roughens layer depth were associated with the ALR site (Table 1). Details about the experimental site and instrumentation can be found elsewhere (Miao et al., 2017).

3.3. Lenoir site (North Carolina, USA)

The agro-forestry experimental site is located in Lenoir County (LEN), on the Lower Coastal Plain of North Carolina, USA. The field is representing an intercropping system of switchgrass (*Panicum virgatum* L.) with loblolly pine (*Pinus taeda* L.). The climate is very similar to ALR with the long-term (1981–2010) mean annual temperature and precipitation obtained from nearby meteorological station (Kinston, NC, National Climatic Data Center, 35.303°, −77.573°) of 16.2 °C and 1264 mm, respectively (Table 1). Soils were classified as Pantego (fine, loamy, siliceous, semiactive, thermic Umbric Paleaquults) or Rains (fine, loamy, siliceous, semiactive, thermic Typic Paleaquults) soil series which are deep, poorly drained, moderately permeable soils. The pine seedlings were planted during winter 2008 on bedded rows spaced 6 m apart and 1.6 m apart within rows at 1075 stems ha^{-1}. Switchgrass (Alamo cultivar) was planted in June 2009 in 3-m-wide alleys with edges approximately 1.5 m away from the rows of pine trees. The observations used in the study were taken between early June till mid November 2015 (Table 1). The maximum height of understory switchgrass reached ~2 m m while the height of overstory pines to ~7.2 m. The plant area index was measured by ACCUPAR LP-80 ceptometer (Decagon Devices, Inc., Pullman, WA, USA). The area averaged PAI reached to ~4 m^2 m^{-2}. The 9 m tall guyed tower with instruments for micrometeorological measurements were deployed near the center of a rectangular-shape field with a length of 120 m and width of 80 m. The field is a part of a larger experimental area (~ 1 km^2) consisting of three types of plots with switchgrass, pines and the pine-switchgrass intercrop. Therefore, despite the micrometeorological measurements are fetch-limited, the surrounding area is of similar landcover mixture. The fetch limitations were also the main reason

why the measurements where kept close to the canopy top. More details about the experimental site and instrumentation can be found elsewhere (Tian et al., 2017).

3.4. Temperature measurements and data pre-processing

At all 3 sites, unshielded fine wire (75 μm) chromel-constantan (type E) thermocouples (OMEGA Engineering, Norwalk, CT, USA) were used for recording long-term high-frequency air temperature measurements. The raw 10 Hz data were collected with a CR1000 dataloggers equipped with a compact flash module CFM 100 and 2 GB compact flash card (Campbell Scientific Inc., Logan, UT, USA). Frequency attenuation was corrected in wavelet space using continuous (Morlet) wavelet transform (Torrence and Compo, 1998). The choice of wavelet analysis method reflects acceptable trade off in locality between time and frequency domains. The wavelet spectrum was computed and the inertial subrange scaling checked. We assumed no sensor attenuation at $f < 0.1$ Hz. After this frequency cutoff, whenever the spectral decay is steeper than −5/3, the wavelet coefficients were adjusted to follow a decay of −5/3. Hence, only the amplitudes were adjusted and the phases were considered to remain unaltered by the sensor. We further assume that at $f > 1$ Hz the only possible decay is −5/3. This lead to a removal of noise (associated with a 'flat' or 'white' spectrum) at the highest frequencies. This approach was preferable than fitting the first order-linear response transfer function in the time domain because the shape of the transfer function lead in some cases to overestimation at high frequencies. We also preferred to use this approach than just consider that the frequency response is not changing with environmental conditions such as wind speed. The adjustment resulted in median 0.1, 0.12, 0.05 s time constants, for POL, ALR and LEN site, respectively. The outcome of this approach was verified by comparing temperature spectra from a 13 μm thermocouple at the LEN site (SI 2). To remove the very low-frequency motion related to meso-scale events and not contributing to H, filtering the low frequency wavelet coefficients was performed. This filtering ensured that the second order structure functions at scales exceeding the inertial subrange do not show any significant trends (SI 3).

The pre-processed time series of air temperature were used to compute σ_T and S_T following Tillman (1972), and a with $d+s$ following Van Atta (1977).

3.5. Sensible heat flux computation, the methods cross-comparison and evaluation

The basic procedure of computing H from FV follows most of the approaches introduced in the theory Section 2. These included (i) a free convection version of FV according to Eq. (8); (ii) an iterative solution of Eq. (6) with 2D wind speed measurements using an expression for integrated wind profile (Paulson, 1970; Högström, 1988; Grachev et al., 2000, 2007) with an adaption for the measurements in the RSL (De Ridder, 2010) in the case of ALR and LEN; and (iii) the Eq. (6) with L_O directly determined from EC measurements.

Several variants of the SR method were tested. They encompassed (i) traditional VA solution of the scale I together with Eq. (21); (ii) the more recent VA solution of the scale II according to Shapland et al. (2012a) and Eq. (21) yet assuming that $\alpha \approx 1$; (iii) SR combined with dissipation method following Eq. (28); (iv) the free convection version obtained from Eq. (41) with ξ set $-\infty$ and where importantly, ϕ_h scales with $\xi^{-1/3}$ as described by Grachev et al. (2000); (v) an iterative solution of Eq. (27) with 2D wind speed measurements using an integrated wind profile in a identical manner as described above for FV; and (vi) SR expression from Eq. (27) with a directly determined L_O and u_* from EC measurements.

The sensible heat flux from combined FV-SR methods was determined through (i) a linear regression fitting of the χ dependence on ξ in a log–log space; or (ii) a numerical optimization of χ to ξ relations for each half-hour by minimizing the difference in EC-based ξ and ξ as a double-log-linear function of χ using evolutionary global optimization via the differential evolution algorithm (Ardia et al., 2011). The obtained parameters were averaged across the three sites to provide generalized forms allowing to estimate ξ and subsequently H through Eqs. (6) or (38) whose outcomes can be either treated individually or averaged.

Since the measurements at ALR and LEN sites were performed in the RSL, z^* is needed to replace $z-d_0$ by z^*-d_0. An approach of maximum simplicity was adopted with $z^* = h+15z_o$ where $z_o = 0.29(h-d_0)$ is the roughness length for momentum (Verhoef et al., 1997; Hall, 2002). To account for the dependency of d_0 on canopy density, a relation between d_0 and PAI from Shaw and Pereira (1982) were adopted.

The EC method was used as reference for evaluation of FV and SR. The raw EC data were collected at datalogging unit LI-7550 (LI-COR Inc., Lincoln, NE, USA) and consisted from H_2O concentration measured either by a LI-7500 or LI-7200 (LI-COR Inc., Lincoln, NE, USA) for POL and ALR, respectively. Sonic temperature and wind component were measured by 3D sonic anemometer Gill WindMaster (Gill Instruments Ltd., Lymington, UK) at all three sites and temporarily (2016-06-14 to 2016-09-01) by CSAT3 (Campbell Scientific Inc., Logan, UT, USA) at the ALR site. The EC fluxes including H were determined using an open source software EddyPro (LI-COR Inc., Lincoln, NE, USA) and with widely adopted set of corrections and subsequent data screening criteria. In the case of LEN, no high-frequency H_2O and thus no EC LE measurements were available and the Schotanus et al. (1983) correction was omitted leading potentially to a minor overestimation of H. To evaluate EC energy balance closure, the sum of H and LE was compared against the difference between net radiation (R_n) and soil heat flux (G) at POL and ALR sites with full EC setup. To measure R_n, NR01 (Hukseflux, Delft, the Netherlands), CNR4 (Kipp & Zonen, Delft, the Netherlands), and Q7.1-L (REBS, Seattle, WA, USA) net-radiometers were used at POL, ALR, and LEN sites, respectively. At POL site, G was measured by pairs of HFP01 sensors (Hukseflux, Delft, the Netherlands) installed at ~5 cm depth, while pairs of HFT3-L (REBS, Seattle, WA, USA) were used at ALR (~2 cm depth) and LEN (~5 cm depth) sites, respectively. Except for the EC post-processing performed in EddyPro, all data processing, analyzes, and graphical presentation were performed with R Statistical Software (R Core Team, 2023) using our own scripts for consistent data treatment across the sites. Sample R codes to perform the analyses presented in this study are available at https://github.com/MilanFischer/FV-SR_methods.

4. Results

The results section begins by addressing the connection of FV and SR to ξ and universal stability functions. This introductory part is followed by an evaluation of different FV and SR schemes including the free convection limit and schemes requiring wind velocity measurements. Since some of these schemes are dependent on ξ, potential approaches how to predict ξ are also considered. Finally, a novel approach resulting from the combination of FV and SR and their mutual constraints is introduced and evaluated.

4.1. Integral turbulence characteristics of temperature

The normalized standard deviation of temperature scaled with stability at all the three sites is shown in Fig. 1. The fact that the predicted free convection limit fits the measurements at a wide range of unstable stability conditions and within the RSL suggests that a $z^*/h = 2$–3 is plausible. Moreover, it justifies its incorporation into the MOST relation in lieu of z for the cases when measurements are conducted in the RSL. As expected, there is an obvious difference in the explained variability by the universal stability function for unstable and stable conditions, where the latter is more uncertain. This has several implications for estimating H under stable stratification as will be evidenced later.

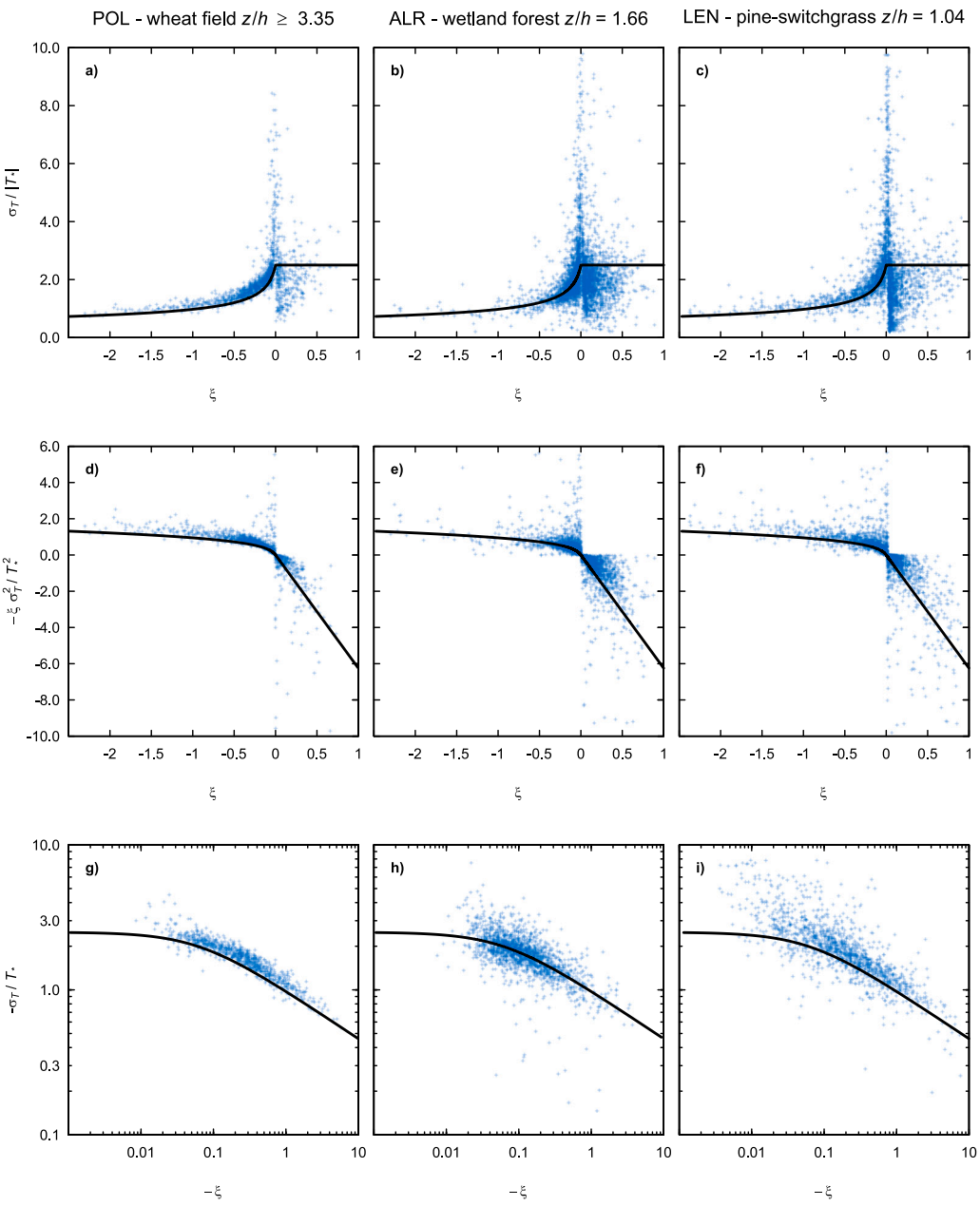

Fig. 1. Analyzes of the air temperature variance dependencies on the stability parameter ξ across the 3 sites (columns) including Polkovice (POL), Alligator River (ALR) and Lenoir (LEN) site. The solid black line depicts the prediction (Eq. (7) for $\xi < 0$ or constant for $\xi > 0$) using the original parameterization by Tillman (1972). Note that this prediction deviates from measurements especially under near neutral and stable atmospheric stratification (a–f). I.e. conditions under which either the instrumental errors dominate (neutral stratification) or MOST assumptions become violated (very stable stratification). The bottom row presents the normalized standard deviations for unstable conditions on a double-log curve to emphasize the free convective scaling $(-\xi)^{-1/3}$ (d–i). The height $z - d_O$ is replaced by $z^* - d_O$ in the RSL ($\sim z/h < 3$). The values of aerodynamic properties are listed in Table 1.

Close to the neutral conditions, σ_T is small but finite while T_* is near-zero resulting in large uncertainties when computing $\sigma_T/|T_*|$. It is to be noted that σ_T is far more impacted by sensor noise compared to $\overline{w'T'}$ under near-neutral conditions, which explains the anomalous large values in the near-neutral stability regime. Nonetheless, from the perspective of FV applications, these relations are useful for calibrating z^* and examining the validity of the main assumptions in FV. Fig. 1 suggests that the C_3 constant might differ from those found in the literature. This is discussed in Tillman (1972) who attributed the reason of discrepancy to the surface heterogeneity and confirmed in other studies (Katul et al., 1995; Waterman et al., 2022). Again, surface heterogeneity impacts the variances more than the turbulent fluxes as individual variances (surface + air turbulence) are always additive.

4.2. The dependence of SR parameter α on stability

The parameter α exhibited dependency on atmospheric stability with higher and lower values reported for unstable and stable cases, respectively (Fig. 2a–c). The asymptotic behavior is reasonably described by the approach proposed by Castellví (2004) and the alternative derivation from this study (Fig. 2d–f). The best agreement in α derived from measurements of ramp statistics and H and their predicted counterpart was found in the ASL. When comparing the parameter α determined from measurements with that determined from the stability parameters, the predictions overestimate the small values and underestimate the high values (Fig. 2g–i). Nevertheless, the implication for the H determination is less pronounced as evident from further evaluation. Similar to FV, from the perspective of SR applications, these relations

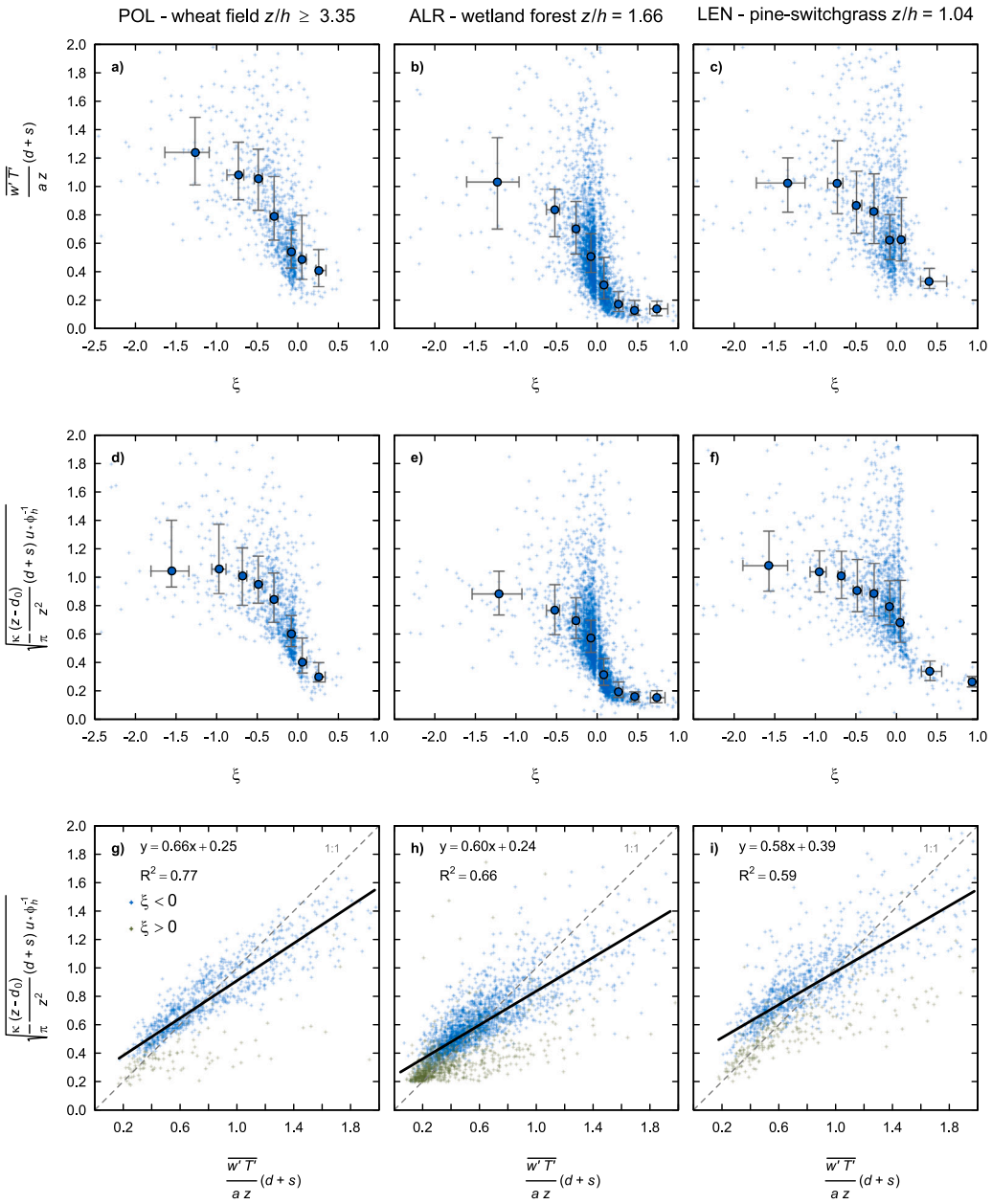

Fig. 2. Analyzes of the SR parameter α and its dependency on the atmospheric stability parameter for the ASL and RSL. The parameter αz can be interpreted as the mean volume of air per unit ground area exchanged on average through ramp-cliff coherent structures, or as the mean effective eddy size associated with these structures. Top panel (a–c) shows α derived from direct EC measurements while middle panel (d–f) the predictions based on Eq. (27) (Castellví, 2004) which is equivalent to the derivation proposed in this study (Eq. (38)). Since the α parameter is not dependent only on the stability parameter ξ but also on u_*, the binned medians (with the error bars representing the 25th and 75th quantiles) are presented to clearly visualize the stability dependence (a–f). The comparison of the α estimated from direct measurements and the predicted counterparts is provided for both unstable (blue points) and stable (green points) atmospheric stratification (g–i) along the one-to-one gray dashed line, linear fit (black solid line) and the regression statistics.

can be employed for calibrating z^* and examining the validity of the main assumptions in the SR expression.

4.3. The SR approach relying only on the air temperature measurements

Testing of the SR expressions that are not dependent on the stability parameter did not show any consistent behavior of the α parameter and provided relatively large scatter (Fig. 3). The parameter α determined from the so called scale I SR approach ranged from 0.52 to 0.69 in the case of unstable cases. It ranged from 0.15 to 0.36 in the case of stable cases (Fig. 3a–c). The scale II SR approach assumes that the parameter $\alpha \approx 1$ and does not require any calibration. However, the results here suggest that α varied from 0.93 to 1.42 (Fig. 3d–f. Moreover, they indicate that the scale I SR approach provides higher coefficient of determination (R^2) when compared to scale II SR and thus a calibrated scale I SR might be more accurate for practical purposes.

Besides the two approaches relying solely on the ramp characteristics, a method proposed by Castellví and Snyder (2009) based on a combination of SR with the dissipation method (Hsieh et al., 1996; Hsieh and Katul, 1997) requiring additionally the measurement of temperature variance was tested (Fig. 4). At all three sites, this method experienced a large overestimation of H, which was the most pronounced in the case of ALR and the least pronounced in the case of POL.

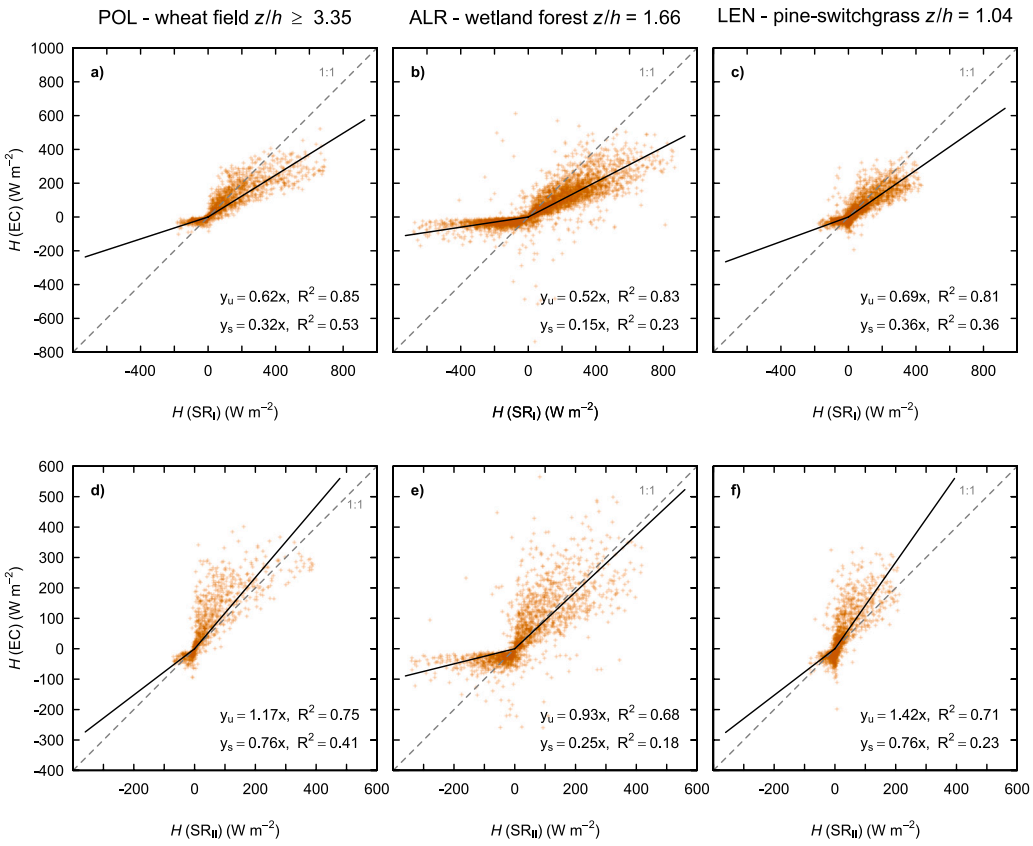

Fig. 3. Evaluation of the SR schemes for scale I (a–c) and II (d–f). In both schemes, Eq. (21) was used to derive H but the time lags (r) needed to resolve Eqs. (19) and (20) differed. While in the case of scale I, r represents the first local maximum of the absolute value of cubic structure function divided by r, in the case of scale II, r is set to gradual rise period (d) resulting from the scale I ramp characteristics (Shapland et al., 2012a,b). Note that the EC measured H is the ordinate whereas the SR predicted H is the abscissa. Thus, the slope of the linear regression can be interpreted as the α parameter (or corrections to it). The regression statistics (with linear fit by black solid line) associated with this comparison along with the one-to-one gray dashed line are also shown.

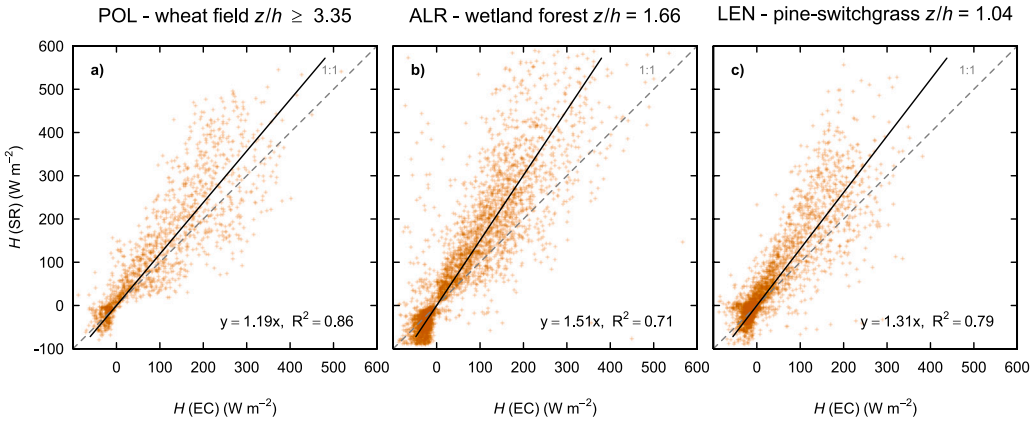

Fig. 4. Evaluation of the SR scheme based on the combination with dissipation method (Eq. (28)) as proposed by Castellví and Snyder (2009). The parameter G_k was set to 1.66 for unstable cases as originally suggested by Hsieh et al. (1996) but to 0.8 for stable atmospheric stratification cases resulting from an analysis of the MOST functions. The regression statistics (with linear fit by black solid line) associated with this comparison along with the one-to-one gray dashed line are also provided.

4.4. FV and SR under free convection conditions

The operational use of the free convection limit of FV has been reasonably established for predicting H using measured σ_T (Albertson et al., 1995; Tillman, 1972). This is because of the term $(\phi_T|\xi|^{1/3})^{-3/2}$ resulting from Eq. (6) decreases rapidly towards unity with increasing $-\xi$ and becomes constant. In contrast, a free convection limit of SR is less straightforward. An approximation of free convection version of SR was also proposed (Castellví, 2004) as an expression resulting from a typical value of ϕ_h for ξ within −3 to −0.03. The main reason for the lack of well determined limit is an application of Kansas based ϕ_h that scales with $(-\xi)^{-1/2}$ contrary to MOST under unstable atmospheric stratification. As a consequence, the term $|\xi|^{-1/4}\phi_T^{-1/4}\phi_h^{-1/2}$ from the Eqs. (40) and (41) does not converge to a constant value with increasing $-\xi$. In this study, a formulation of ϕ_h that scales correctly with stability for $\xi \ll -1$ with an exponent of −1/3 instead of −1/2 (Grachev et al., 2000) is used and thus allows for an explicit derivation of a free convection SR version. A comparison of free convection expression for both FV and SR is provided in Fig. 5 for unstable conditions. These comparisons yield high coefficients of determination ($R^2 > 0.93$) for

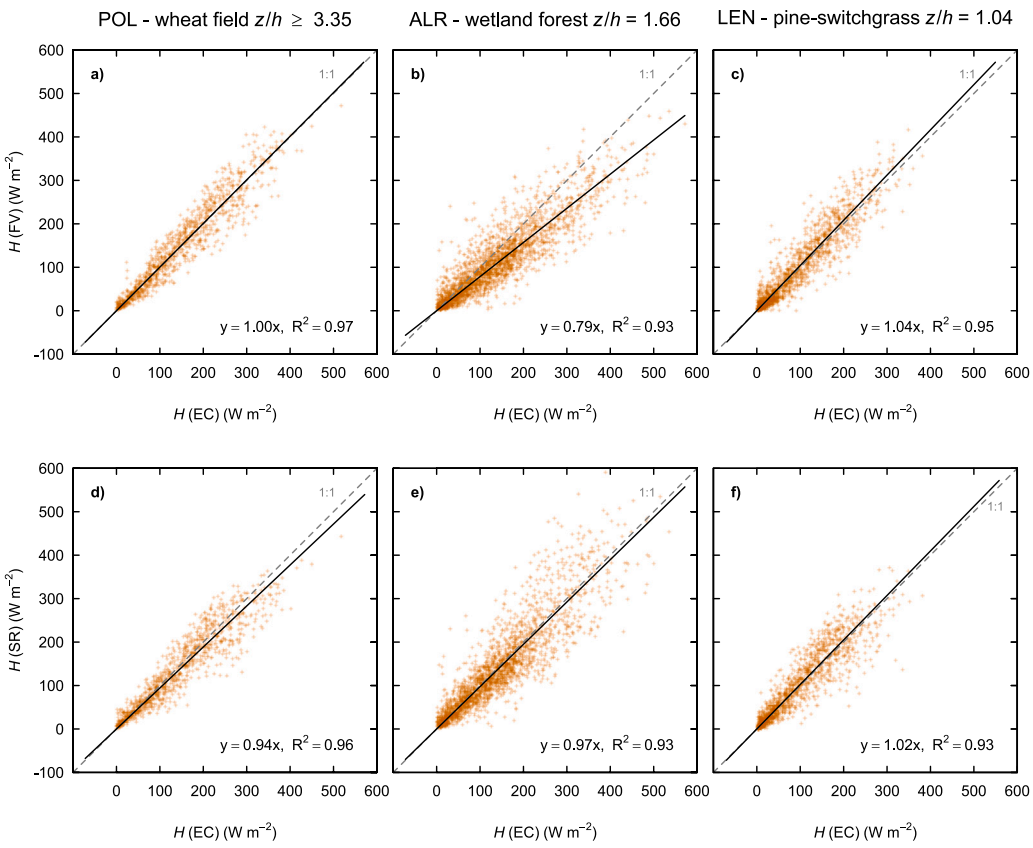

Fig. 5. A comparison between H measured by EC and H predicted using FV (a-c) and SR (d-f) when employing the free convection scaling with the EC measurements. The free convection approximation was obtained by setting $\xi \to -\infty$ in Eq. (6) (FV) and Eq. (41) (SR). To facilitate explicit determining free convection form of SR, we used the function for ϕ_h proposed by Grachev et al. (2000) as it obeys MOST in the free convection limit. The regression statistics (with linear fit by black solid line) associated with this comparison along with the one-to-one gray dashed line are also shown.

both methods and for ASL and RSL flows. While R^2 is marginally greater in the case of FV, the slopes are closer to unity in the case of SR (0.94–1.02) as compared to FV (0.79–1.00). It is evident that the stability at ALR is represented by more frequent near neutral conditions (Fig. 2) and hence the free convection limits are sporadically achieved. Interestingly, in terms of regression slopes, SR showed less sensitivity to the violation of not being in free convection compared to FV.

4.5. FV and SR for entire stability range with additional wind velocity measurements

When the high-frequency air temperature measurements are combined with horizontal wind speed measurements, an iterative approach can be used to determine H, u_* and L_O for the entire stability range. An evaluation of this approach of FV and SR against EC is provided in Fig. 6. Although FV yielded higher R^2 for all three measurement setups, SR resulted in higher agreement with EC in terms of slopes that were within a few percent from unity (0.94–1.06). FV differed from EC and showed some inconsistent behavior with overestimation for POL (1.11) and LEN (1.08) and underestimation for ALR (0.81).

To provide a 'proof of concept' evaluation of the system of equations involved in FV and SR, we used u_* and L_O measured by EC to determine H by FV and SR methods and compared them against H from EC (Fig. 7). In terms of linear regression slopes, this comparison provided minor improvements for FV and SR with EC as compared to the comparison presented in Fig. 6. The coefficients of determination were slightly lower in the case of FV and slightly higher in the case of SR. As in the previous comparison, the regression slopes were closer to unity in the case of SR (0.98–1.04) as compared to FV (0.95–1.15).

The incorporation of u_* and L_O measured by EC to determine H using the FV and SR methods was additionally used for evaluating the widely used stability correction functions to explore the sensitivity of H to their different forms (Tables 2 and 3). It is obvious that the selection of the stability correction function is significant for deriving H using both the FV and the SR methods. However, this analysis also suggests that the SR scheme is less sensitive to the choice of MOST function as compared to FV. The analysis further suggests slightly better performance of SR under stable stratification compared to FV which performance under stable conditions was rather inferior. The most reliable FV results under stable atmospheric stratification were obtained by applying the Kansas parameterization of $C_3 = 1.77$ (Tillman, 1972) while increasing C_3 led to their deterioration.

The regression analysis of EC measured H and LE against $R_n - G$ yielded an energy balance closure of 0.74 ($R^2 = 0.97$) at the POL and 0.84 ($R^2 = 0.93$) at the ALR sites. Note that it was not possible to determine the energy balance closure at the LEN site where LE was not measured. To address the potential impacts of EC energy balance closure on the evaluation of FV and SR using EC measured u_* and L_O, three simplified energy balance closure scenario were considered. The first scenario assumes that all the energy balance residuum is assigned to LE and thus H remains unaltered. The second scenario assumes that the energy balance residuum is distributed to both H and LE in a way that the Bowen ratio, i.e. H/LE, is conserved. The third scenario assumes that the entire energy balance residuum is assigned to H and consequently LE remains unaltered. The outcome of the first scenario was already presented (Fig. 7) and serves as a reference. In the case of the second scenario, the slopes of regression between FV, SR and EC decreased from the reference values of 1.15 and 0.98 for FV and SR, respectively (Fig. 7), to 0.83 ($R^2 = 0.95$) and 0.71 ($R^2 = 0.93$) for the POL site, and from 0.95 and 1.04 to 0.76 ($R^2 = 0.85$) and 0.84 ($R^2 = 0.86$) for the ALR site. In the case of the third scenario, the regression

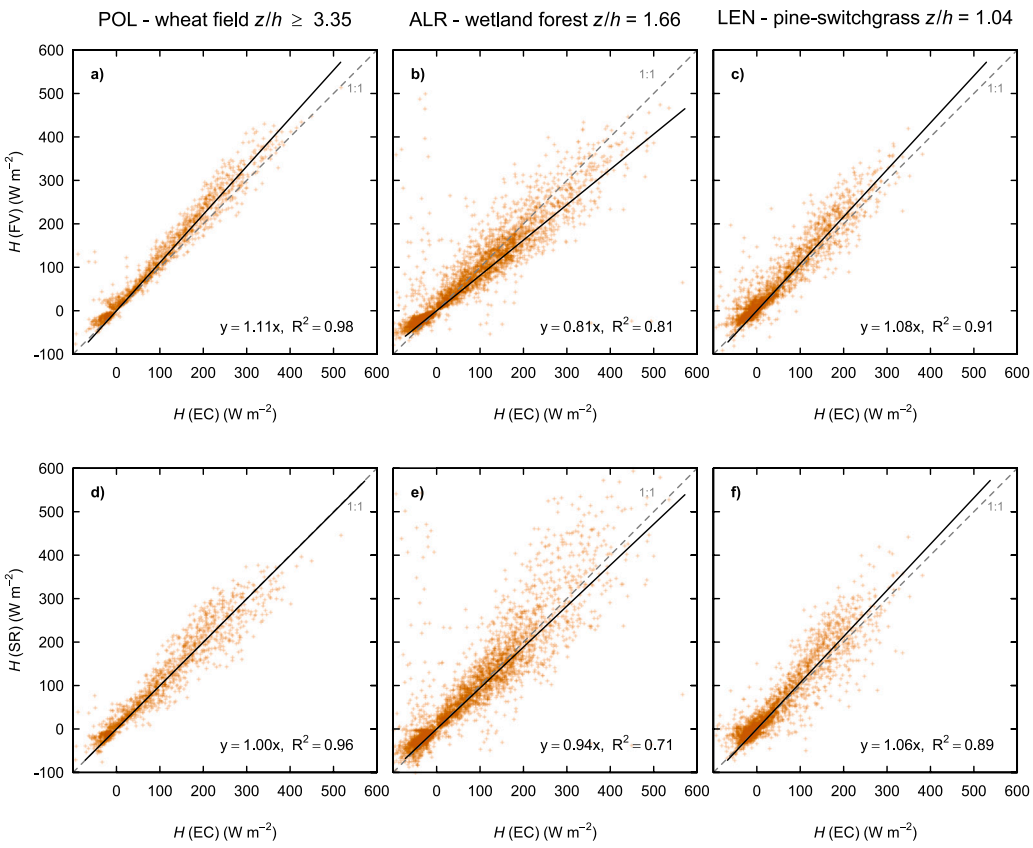

Fig. 6. A comparison of H measured by EC and H predicted by FV (a-c) and SR (d-f) within the scheme that uses mean horizontal wind speed measurements along with an iterative approach using the integrated wind profile (Paulson, 1970; Högström, 1988; Grachev et al., 2000, 2007) adjusted for the measurements in RSL (De Ridder, 2010) in the case of ALR and LEN sites. The calculation of H by FV followed Eq. (6) with the original parameterization by Tillman (1972) while the calculation of H by SR used Eq. (27) with parameterization by Grachev et al. (2000) and Grachev et al. (2007) for unstable ans stable stratification, respectively. The associated regression statistics (with linear fit by black solid line) along with the one-to-one gray dashed line are also shown.

Table 2
The impacts of selected different forms of the empirical MOST functions on errors in H statistics when FV (Eq. (6) is compared to EC. The slopes of linear regression (m) with intercept forced to zero and the associated coefficients of determination (R^2) are provided.

MOST function	POL		ALR		LEN	
	m	R^2	m	R^2	m	R^2
unstable						
Tillman (1972)	1.16	0.98	0.96	0.91	1.16	0.90
Foken et al. (1991) and Foken (2008a)	1.17	0.98	0.96	0.92	1.16	0.92
Kaimal and Finnigan (1994)	1.34	0.98	1.15	0.91	1.35	0.90
Maronga and Reuder (2017)	1.23	0.98	1.05	0.90	1.22	0.88
stable						
Tillman (1972) with $C_3 = 1.77$	0.82	0.33	0.87	0.31	0.67	0.22
Tillman (1972) with $C_3 = 2.5$	0.45	0.19	0.50	0.17	0.37	0.10
Sorbjan (1987) with $C_3 = 3.5$	0.20	0.05	0.25	0.06	0.16	0.03
Foken et al. (1991) and Foken (2008a)	0.45	0.22	0.51	0.16	0.39	0.21
Kaimal and Finnigan (1994)	0.68	0.22	0.80	0.26	0.56	0.13
Pahlow et al. (2001)	0.17	0.04	0.22	0.04	0.11	0.01

slopes decreased further to 0.73 (R^2 = 0.93) and 0.63 (R^2 = 0.92) for the POL site, and to 0.60 (R^2 = 0.79) and 0.64 (R^2 = 0.79) for the ALR site. Overall, the application of the second and third energy balance closure scenario deteriorated the agreement between FV, SR and EC.

4.6. Approximating the stability parameter from air temperature statistics

In convective boundary layers, the S_T correlates with ξ and can be used as the stability parameter predictor (Tillman, 1972). This conjecture was tested for both unstable (Fig. 8a-c) and stable (Fig. 8d-f) stratification. Beside that, we tested the ratio of non-random (coherent) variance to the entire variance determined by Lorenz thresholding of wavelet coefficients (Katul and Vidakovic, 1996) as an alternative predictor of ξ. The rationale was inspired by Katul and Vidakovic (1996) who showed that the number of wavelet coefficients representing the turbulent eddies increases with stability since the vertical velocity is simultaneously dampened by the ground and density stratification. Similarly, we propose that the ratio of non-random (coherent) variance to the entire variance increases with $-\xi$. Although a significant relations between the selected predictors and ξ were found (Fig. 8), the uncertainty of such approach is large making it unsuitable for operational predictions of H.

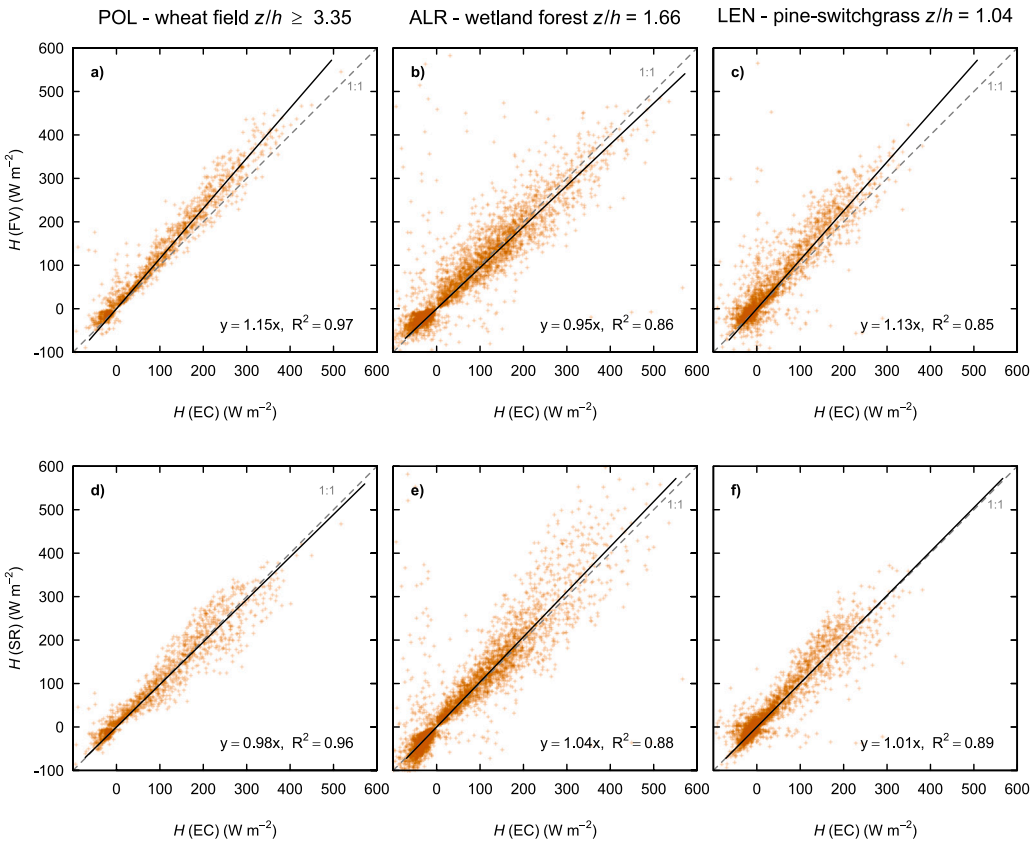

Fig. 7. An examination of H derived through FV (a-c) and SR (d-f) where u_* and L_O were determined directly by a 3D sonic anemometer. The calculation of H by FV followed Eq. (6) with the original parameterization (Tillman, 1972) while the calculation of H by SR used Eq. (27) with the parameterization covering wide range of atmospheric stability (Grachev et al., 2000, 2007). The regression statistics (with linear fit by black solid line) associated with this comparison along with the one-to-one gray dashed line are also shown. Note that for consistency with prior analysis, the sign of H was inferred from cubic structure function for both methods rather than directly inferred from L_O.

Table 3
The impacts of selected different forms of the empirical MOST functions on H error statistics when SR (Eq. (27)) is compared to EC. The slopes of linear regression (m) with intercept forced to zero and the associated coefficients of determination (R^2) are provided.

MOST function	POL		ALR		LEN	
	m	R^2	m	R^2	m	R^2
unstable						
Högström (1988)	0.99	0.97	1.03	0.93	1.05	0.93
Foken et al. (1991) and Foken (2008a)	0.98	0.97	0.98	0.93	1.06	0.93
Kaimal and Finnigan (1994)	1.02	0.97	1.06	0.93	1.09	0.93
Grachev et al. (2000)	0.98	0.96	1.05	0.92	1.03	0.92
stable						
Högström (1988)	0.48	0.42	0.66	0.21	0.44	0.33
Beljaars and Holtslag (1991)	0.52	0.44	0.72	0.23	0.48	0.35
Foken et al. (1991) and Foken (2008a)	0.54	0.46	0.73	0.25	0.49	0.34
Kaimal and Finnigan (1994)	0.51	0.44	0.72	0.24	0.47	0.35
Chenge and Brutsaert (2005)	0.47	0.42	0.66	0.21	0.44	0.33
Grachev et al. (2007)	0.54	0.45	0.75	0.24	0.50	0.36

4.7. Combining FV and SR methods

The last approach to be tested is combining the FV and SR methods. The first analysis was focused on investigating the behavior of the quantity χ versus ξ. Given the nature of Eq. (42), this quantity shows highly nonlinear behavior at all sites and stability conditions. To allow an analytical solution of the system of equations, the log-linear relation between the stability parameter ξ and the quantity χ was explored (Fig. 9).

It is evident that the dependence of χ on ξ is site specific, especially in stably stratified cases (Fig. 9). Therefore, site-specific fits or, more preferably, one general fit can be used to obtain ξ from χ obtained from measurements and subsequently H. Using the derived least-squares fit across all three sites (red solid line in Fig. 9 and the parameters P5–P8 labeled as "all" in Table 4) provides reasonable estimate of H for both unstable and stable conditions (Fig. 10). The resulting form for predicting ξ from combined FV and SR using the right-hand side of the Eq. (42) $\chi = \kappa(z-d_0)/(\pi^2\, g(d+s)^2)\, T a^4 \sigma_T^{-5}$ to be applied in conjunction with Eqs. (6) or (38) to predict H follows as (with sign of ξ from SR)

$$\xi = \frac{-\chi^{(1/P6)}}{e^{(P5/P6)}} \text{ if } \xi < 0;\ \xi = \frac{\chi^{(1/P8)}}{e^{(P7/P8)}} \text{ if } \xi > 0\,. \tag{43}$$

Due to the different formulation of the dependency of H on ξ in FV and SR, the choice of either Eq. (6) or Eq. (38) will lead to slightly different result. For practical purposes, one may select the one which

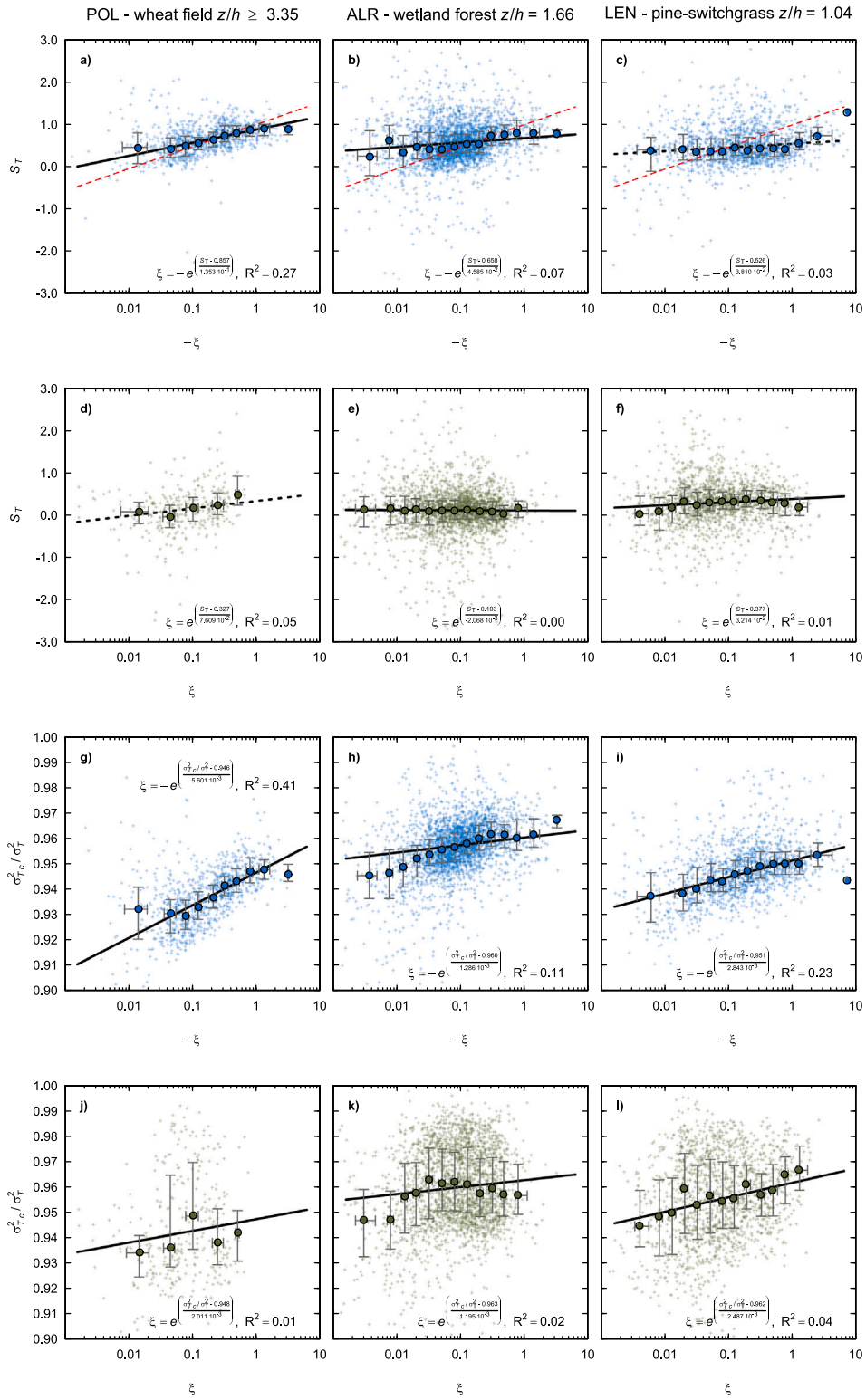

Fig. 8. An approximation of ξ as a function of air temperature skewness S_T (a–f) and fraction of temperature variance associated with coherent eddies $\sigma^2_{T_c}$ related to overall variance σ^2_T (g–l). The solid black lines depict the statistically significant ($p \leq 0.05$) relation, while the dotted black lines depict the insignificant ($p > 0.05$) relation. The thin dashed red line represents the original expression (Tillman, 1972) for unstable atmospheric stability conditions (a–c). To visually emphasize the main pattern, the binned medians (with the error bars representing the 25th and 75th quantiles) are provided.

is leading to better agreement with EC, or use the average of both. Results with negligible differences were obtained when matching FV and SR (Eqs. (6) and (38)) was carried out through computationally more intensive iterative optimization minimizing the difference in H between FV and SR. Further analysis revealed that these parameterizations are useful only for solving H and not u_* or L_O. In fact, the fitted relations suggest the importance of ξ within the range of −1 to 0.1. In stable cases, one single value of ξ close to 0.3 can be perhaps

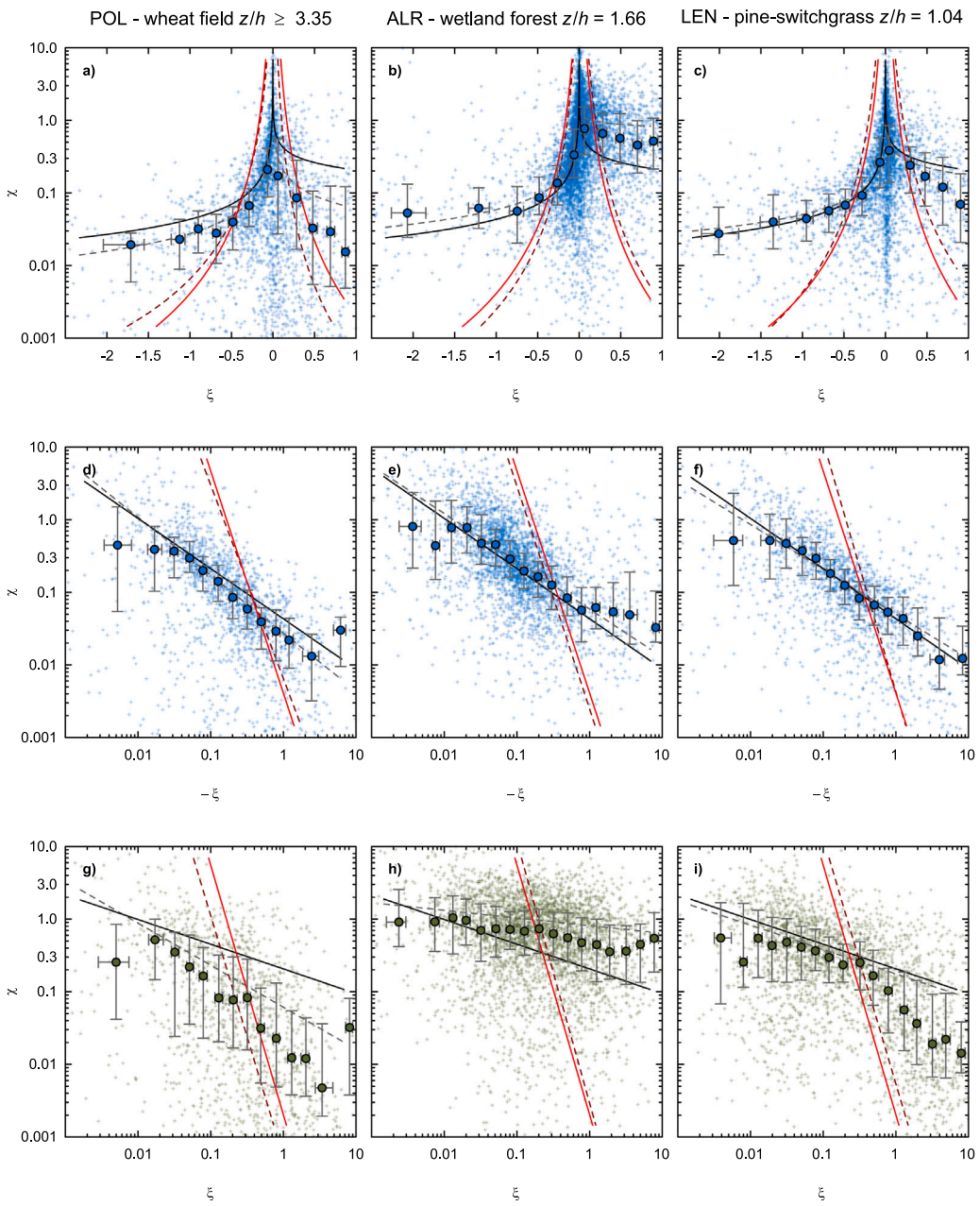

Fig. 9. The relation between χ obtained by combining FV and SR methods (Eq. (42)) and the stability parameter ξ in a semi-log (a–c) and log–log visualization for unstable (d–f) and stable cases (g–i). The gray dashed line is a site-specific fit, while the solid black line is a mean fit across all sites in log–log space. The dark red dashed line originates from optimization minimizing the difference between EC measured and predicted ξ at each site, while the solid red line represents the mean of these fits across all the three sites. To highlight the main patterns, the binned medians (with the error bars representing the 25th and 75th quantiles) are provided.

used. The comparison with EC measured H yielded R^2 within 0.88–0.97 and regression slopes within the range of 0.93–1.04 (Fig. 10). These basic statistics are suggestive that the combined approach yields H predictions commensurate with those of FV and SR methods used separately but supplemented by u_* and L_O measured by EC.

5. Discussion

5.1. The historical context of FV and SR

Some 30 years after Higbie (1935) introduced the SR theory to predict mass exchange, Brutsaert (1965) extended this approach to the evaporation of rough surfaces. The working assumption in Brutsaert (1965) is that micro-scale eddies are responsible for much of the mass (or heat) exchange between the surface and the atmosphere. A plausibility argument supporting this assumption is that micro-eddies still carry sufficient energy for impinging and transporting scalars and their collision frequency with the surface far exceeds their large-scale counterparts even though the energy content of large-scale eddies is much larger (Katul and Liu, 2017). In 1972, Tillman initiated an entirely different line of inquiry to estimate turbulent fluxes from variances of scalar time series measurements. A method based on MOST FV relations was then proposed and explored over many sites and studies (Albertson et al., 1995; Guo et al., 2009; Kotani and Sugita, 2007; French et al., 2012). Some three decades after Brutsaert's work, Paw U and collaborators (Paw U and Brunet, 1991; Paw U et al., 1995; Snyder et al., 1996) proposed a new approach that combines the phenomenology of SR (Higbie, 1935) with the much-discussed ramp-cliff patterns associated with coherent structures in boundary layers and canopy sublayers (Gao et al., 1989; Paw U et al., 1992). The present

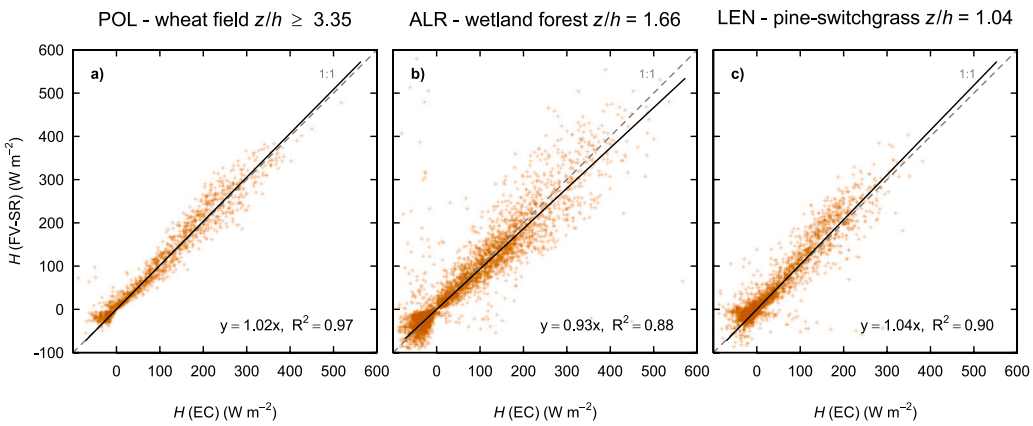

Fig. 10. Comparison between H measured by EC and H predicted using the combined FV-SR scheme. The prediction is based on the parameters P5–P8 labeled as "all" (Table 4) and Eqs. (42) and (43) to estimate ξ which is then used as input to FV Eq. (6) (parameterization by Tillman, 1972) and SR Eq. (38) (parameterization by Grachev et al., 2000 and 2007) and the result from both is subsequently averaged. Note that the combined approach requires only high-frequency air temperature measurements. The regression statistics (with linear fit by black solid line) associated with this comparison are also shown along with the gray dashed one-to-one line.

Table 4
The empirical fitting parameters allowing to predict the stability parameter ξ from the quantity χ resulting from the analysis in Fig. 9. The parameters P1–P4 originates from the fit between χ and ξ (gray and black lines in Fig. 9) while the parameters P5–P8 originates from optimization minimizing the difference between EC measured and predicted ξ (red lines in Fig. 9). The columns include site-specific parameters for each of the three sites as well as a combined set of parameters under the column labeled as "all".

	POL	ALR	LEN	all
unstable				
P1	−3.60	−2.84	−2.99	−3.14
P2	−0.80	−0.66	−0.62	−0.69
stable				
P3	−2.79	−0.21	−1.73	−1.58
P4	−0.58	−0.11	−0.34	−0.34
unstable				
P5	−5.03	−6.00	−5.45	−5.50
P6	−2.66	−3.07	−3.44	−3.06
stable				
P7	−7.55	−5.83	−5.22	−6.20
P8	−3.33	−3.60	−3.38	−3.44

study evaluates both of these approaches, i.e. FV and SR methods, and further investigates how they can be combined.

The newer, which we label "macroscopic", SR scheme proposed by Paw U and Brunet (1991) and Paw U et al. (1995) departs from Higbie's conventional SR theory in multiple ways: (i) it assumes that coherent structures, not micro-scale eddies, are responsible for much of the mass and heat exchange, and (ii) it employs Eulerian high-frequency measurements of scalar concentrations or air temperature to infer ramp statistics in lieu of probabilistic models for contact duration of parcels of air with the surface. The dominance of micro-scale eddies in the turbulent transport as described by Brutsaert (1965) appears to contradict the dominance of large eddies, i.e. coherent structures, according to Paw U et al. (1995). Nevertheless, these two views are not necessarily contradictory. An illustrative explanation of this statement has been given by Moog and Jirka (1999) suggesting that turbulent SR can be envisaged as a circular chain saw cutting a tree. The small teeth on the saw (eddies commensurate with Kolmogorov microscale) perform the actual cutting, while the larger saw blade (large eddies—coherent structures) carries them to and from the cutting zone. Both the speed of the chain and the frequency with which the blade takes swipes at the cutting zone control the cutting. The small eddies resemble the teeth, while the large eddies resemble the swipes, and both control the transport of heat from the surface to the atmosphere. In this context, the approach by Brutsaert (1965) infers the transport from the statistics of microscopic eddies close to the dissipation of their kinetic energy to heat occurring at time scales of microseconds while the approach by Paw U et al. (1995) infers the transport from the statistics of macroscopic eddies close to their production characterized by time scales on the order of tens of seconds. The agreement between these two approaches implies certain coordination between the large and micro-scale transport properties of turbulence: ramp-like structures bring micro-scale eddies to the surface, but heat is exchanged at the surface most efficiently by these micro-scale eddies. After these Kolmogorov micro-eddies remove heat from the surface, heat is then exchanged with the atmosphere through larger-scale eddies. The larger scale eddies are simultaneously transporting the micro-eddies to and from the surface while heat is diffusing within these larger eddies themselves by the velocity field.

5.2. The salient unknown in the SR method

The general drawback of SR is that air parcel volume exchanging heat or scalars is not entirely known (Paw U and Brunet, 1991; Katul et al., 1996), which necessitates calibration. While the initial studies (Paw U et al., 1995; Katul et al., 1996) considered that roughly half of the air volume below the measurement level is heated ($\alpha \sim 0.5$), other studies indicated α parameter close to unity (Snyder et al., 1996; Spano et al., 1997) or even larger (Spano et al., 1997). It should be noted that $\alpha > 1$ may seem to lack a physical plausibility as already pointed out by Chen et al. (1997b). Nevertheless, it may simply suggest that there is another interpretation of α than being a portion of the air volume between the ground and the measurement level renewed during the contact time as originally stipulated (Paw U et al., 1995). Instead of that, the original α parameter can be rather interpreted as a proportionality coefficient informing about what is the air volume being renewed relative to the reference air volume, i.e. the volume between the ground and the measurement level. In this case, $\alpha > 1$ is possible and indicates simply that the volume of air associated with the ramp characteristics (a and $d + s$) is greater than the volume below the measurement level. In other words, the turbulent exchange is dominated by larger eddies relative to z. Indeed, there is no justification to consider that the air volume associated with the ramp characteristics is geometrically limited by the measurement height. Castellví et al. (2002) interpreted the parameter α as the "effective eddy size" responsible for the air parcel renewal. Hence, it is more likely, that the measurement height is representing a center of these effective eddies passing by

and being renewed rather than their top (Castellví and Snyder, 2009). In line with that, one can observe the dependence of α on ξ as in Fig. 2a–f and elsewhere (Castellví, 2004; Suvočarev et al., 2014) with α often exceeding unity with larger growing atmospheric instability while being typically smaller than 0.5 for stable conditions. Castellví et al. (2002) and Castellví (2004) attempted to by-pass the dependency of SR on calibration and constrained the main SR coefficient with MOST using flux-gradient relations. In line with the previous reports (Suvočarev et al., 2014, 2019), an examination of widely used SR approaches conducted here suggested that the constraint proposed by Castellví (2004) appears optimally suited for operational use. Some reservations to the approach proposed by Castellví (2004) have been raised by Shapland et al. (2012b) who commented that this approach aims to relate similarity-derived transfer coefficients valid for longer averaging period (15–30 min) to coherent structures that are generally much shorter. With an intention to provide an SR method that is free from any MOST-based coefficients with not necessarily any strict physical paradigm (Shapland et al., 2012b), an alternative approach has been proposed (Shapland et al., 2012a). This approach assumes that the temperature ramp characteristics themselves contain all the necessary information to determine H and that variability in different α formulations is given by the choice of time lag used to solve the structure functions (Shapland et al., 2012a) and the frequency response of the thermocouples (Shapland et al., 2014). Both of these arguments were discussed in several previous studies in which the dependence of α on the choice of time lag was pointed out e.g. by Snyder et al. (1996), Spano et al. (1997) or French et al. (2012) while the dependence on the thermocouple frequency response was pointed out by Duce et al. (1998). Other studies also reported a dependence of α on z (Snyder et al., 1996; Spano et al., 1997; Shapland et al., 2012c; French et al., 2012; Rosa and Tanny, 2015). In contrast to considering that α is a parameter lumping all these factors, Shapland et al. (2012a) hypothesized that there are at least two dominant scales of coherent structures where the first scale associated with higher frequencies and thus shorter time lags is non-flux-bearing (being in the inertial subrange where local isotropy should weaken the correlation between w' and T') while the second one is associated with slower eddy motion and thus is flux-bearing. Applying the structure function at very short time lags is leading to detection of non-flux-bearing scale I, which is however nearly linearly related to flux-bearing structures associated with the ramp characteristics of the scale II. Therefore, $\alpha < 1$ is needed to infer the fluxes when ramp characteristics are obtained from very short time lags as a correction factor. Nevertheless, if the ramp characteristics of the scale II are available, $\alpha \sim 1$ and does not need further corrections. To determine the scale II ramp characteristics, one needs to determine the gradual rise period of the scale I and use it as a time lag for resolving the scale II. This approach requires that scale I is resolved as precise as possible, and hence thermocouples with negligible frequency response attenuation or spectral corrected measurements are needed (Shapland et al., 2014). This issue was considered here and the frequency response was tested using a very fine-wire thermocouple. The correction procedure proposed by Shapland et al. (2014) was also applied. These investigations here generally do not lend support to the validity of the two scales SR argument by Shapland et al. (2012a) as the comparison with EC demonstrates (Fig. 3d–f). The inferior results by scale II SR method were also reported by others (Suvočarev et al., 2014; Pozníková et al., 2018). On one hand, as already pointed out by Shapland et al. (2012a,b), there is likely multiple flux-bearing scales exceeding the dimensions of scale II. Nevertheless, we also argue that a clear justification for scale I being non-flux-bearing is missing. As pointed earlier, there are situations when α is close to unity even for very short time lags and hence indicates that scale I is flux-bearing (Pozníková et al., 2018). And again, plotting α against ξ in this study and elsewhere (Castellví, 2004; Suvočarev et al., 2014) clearly illustrates that α deviates from unity. An experimentally confirmed success of the method by Castellví (2004) found in this study yet some previous criticism of applying MOST together with ramps events operating at a much shorter time scale has prompted a new look at its derivation. The goal of this new derivation was to reconcile some assumptions that appear incompatible when SR and MOST are linked. While providing a new derivation here, we also explicitly underline that it must be realized that combining MOST with the SR relations is only valid once the ramps are already averaged over extended periods. That is *per se* guaranteed when the VA solution is considered. While the derivation of VA starts with a single ramp, it assumes that these ramps repeat over the averaging interval of mean flow variables (i.e., 30 min). Moreover, fitting the VA model to measured structure functions already averaged over 30 min intervals can only yield averaged ramp statistics that do not reflect a single ramp event.

5.3. Towards the bridge between FV and SR

After the work of Tillman (1972) and Paw U et al. (1995), several studies compared FV and SR (Paw U et al., 1995; Katul et al., 1996; Castellví, 2004; French et al., 2012; Shapland et al., 2012b) yet none attempted to combine these two methods to simultaneously constrain both. The premise is that ramp statistics and overall variances do not contain identical information — but are certainly related by the fact that the flux-bearing ramps also contribute to variances. Contrary to our study and two other prior studies (Katul et al., 1996; French et al., 2012), most of the other studies comparing FV and SR indicated a rather superior performance of SR over FV. We evidenced that if ξ is determined from direct EC measurements, both methods are commensurate in terms of predicting H with minor improvements. This finding prompted a novel approach that combines FV with SR. The proposed approach yields reliable H estimates potentially without a need for calibration and other instrumentation other than one single fast response thermocouple. In brief, this approach is combining information about the coherent structures with the overall variance to obtain heat fluxes in a turbulent atmosphere. Previously, Paw U et al. (1995), Snyder et al. (1996), Spano et al. (2000), Shapland et al. (2012b), Gray et al. (2022) and others suggested that SR based only on temperature measurements can provide reliable H estimates. The work here generally supports this statement with a qualification. The predictions of H based only on the temperature time series requires merging FV and SR. The newly proposed approach shares, at first glance, some similarities with a method proposed by Castellví and Snyder (2009) since it also requires the ramp characteristics and temperature variance as the inputs. Nevertheless, the assumptions and underlying physics is different. The approach by Castellví and Snyder (2009) is based on the combination of SR with a temperature variance dissipation method (Hsieh et al., 1996). Therefore, it relates the ramp characteristics to production term of the variance budget equation (Castellví and Snyder, 2009) and assumes that additional similarity constant can be obtained by relating the normalized standard deviation function for temperature with the dimensionless temperature gradient as $\kappa\,\phi_T/\phi_h$ which over the wide unstable range converges to a value of $G_k = 1.66$ (Hsieh et al., 1996; Hsieh and Katul, 1997). The comparison of the expression proposed by Castellví and Snyder (2009) with EC presented in this study, however, showed large overestimation in mildly unstable conditions (ξ within ~-0.5–0). This is likely because the constant G_k should be reduced from 1.66 to values close to 1.2–1.3 for the near neutral range (Hsieh et al., 1996). Consequently, in contrast to the original intention, the approach by Castellví and Snyder (2009) cannot be considered as fully independent from the stability parameter despite some success reported earlier (Castellví and Snyder, 2009; Gray et al., 2022). If the parameter G_k is not considered as a constant but as a variable dependent on ξ, the correct scaling (slopes of regression against EC close to unity) can be achieved. Nevertheless, the scatter between predicted and EC measured H remains larger than in the case of other stability dependent methods including those proposed here that combine FV and SR. It also appears that the free convection method works more reliably over the entire unstable range and thus may be preferred for operational purposes.

5.4. Study limitations and further opportunities

A few experimental limitations and challenges were identified and elaborated upon here. On the temperature measurement side, the time response of the thermocouples with thickness of 75 μm was not ideal to capture all relevant eddies and to determine the ramp characteristics as well as the temperature variance accurately. To minimize the underestimation of the temperature fluctuation, the dynamic frequency response correction was applied. The choice of the thermocouple thickness can be deemed as a trade-off between the frequency response and durability. While 13 μm thermocouples with high-frequency response usually break within a few days, the 75 μm thermocouples with lower frequency response typically operate for several months up to years. Another potential temperature measurement limitation might be seen in the application of unshielded fine wire thermocouples and potential influence of the radiation load (Laubach et al., 2000). Shielding the thermocouples can distort the turbulent fluctuations and is thus undesirable from this perspective. Anecdotal analysis here as well as other studies (Katul et al., 1997) did not identify any appreciable differences in the low frequency part of spectra between the different thermocouple sizes within the given range as well as spectra of sonic temperature. Also, no evidence appeared that significant differences in the ramp characteristics in between these different sensors exist. For these reasons, the impact of the radiation load on these small diameter thermocouples is negligible for the purpose of FV and SR H determination. The next experimental limitation pertains to heterogeneity at the ALR site. For the application of FV and SR operating in low z/h, especially the uncertainty in h and PAI, and on them all dependent aerodynamic characteristics, are of importance. To partly alleviate this challenge, iterative footprint analysis using LiDAR and LAI remote sensing data was adopted. In fact, this iterative footprint calculation may be a useful tactic for other micrometeorological studies in general. Finally, to minimize the negative impacts of the very small fetch at the LEN site, the micrometeorological measurements were carried out close to the canopy top, similar to other FV and SR studies (Paw U et al., 1995; Chen et al., 1997b; Spano et al., 2000). The challenges to EC measurements for this setup are reasonably known. Close to the canopy top, resolving fine-scale eddies may be restricted by the sonic anemometer path length that averages out their contribution to variances and covariances. Moreover, very close to leaf surfaces, ultrasound echoes from the canopy elements may distort the detection of the sonic wave travel times and hence velocity measurement (Stannard, 1997). The latter effect is routinely flagged by modern sonic anemometers and communicated to the output devise. The former may be indirectly checked using spectral analysis with an emphasis on whether the expected power-law decay of the velocity spectra (i.e. −5/3) are adhered to at high frequencies in the inertial subrange (SI 4). These checks are complemented with application of standard EC quality control and additional visual control that ensure EC data were not compromised in this setup. A plausible explanation as to why an inertial subrange can exist near the canopy top, but not in canonical wall-bounded flows, is also warranted. Unlike wall-bounded flows, flow over canopies is not constrained by the no-slip boundary condition at the canopy top. The mean flow and turbulence are all finite allowing for an extensive inertial subrange to develop even for $z/h \approx 1$ at fine scales. This inertial subrange contributes some 30%–40% of the overall H as discussed elsewhere (Katul et al., 1998b). Moreover, the characteristic eddy size responsible for heat and momentum exchange is commensurate with canopy height (Paw U et al., 1995; Katul et al., 1998b) — which is some two orders of magnitude larger than the sonic anemometer path length. The scale separation between the sonic anemometer path length and the flux-bearing eddies is one reason why inertial subrange scaling laws near the canopy top persist and remain reasonably resolved by the EC method.

Another set of limitations and challenges were related to methodology. It was shown that the choice of the universal MOST function plays a role in the FV and SR performances. The results suggest that FV is more sensitive to the choice of MOST function than SR. The choice of MOST function should be considered in future FV and SR studies and be always reported. The comparison considered EC as the reference despite its known lack of energy balance closure issue — posing a recalcitrant problem in the EC observational network (Foken, 2008b; Mauder et al., 2020; Liu et al., 2021). To address this topic, three scenarios were considered to force closing the surface energy budget. The results suggested that no adjustment of H due to energy balance closure yields the higher agreement between the methods. However, this can just simply mean that FV and SR result in a similar energy balance closure problem as EC. The previous studies applying SR for both H and LE independently from high-frequency EC raw data (Castellví et al., 2008; Suvočarev et al., 2019) reported, compared to EC, higher and nearly fully closed energy balance closure. Unfortunately, the reason why SR should close the surface energy balance better than EC remains the subject of inquiry. The study by Liu et al. (2021) indicated that the non-closure of the surface layer energy balance is associated with the asymmetry of turbulent energy transport caused by coherent structures. Given the fact that previous studies (Castellví et al., 2008; Suvočarev et al., 2019) report on better energy balance closure by SR, we conjecture that FV and SR may provide an opportunity to diagnose which of the closure scenario is more likely when they are applied on independent H and LE measurements from raw high-frequency EC data. At the same time, FV and SR using high-frequency EC data (i.e., sonic temperature and water vapor concentrations) may be used to test the emerging energy balance closure corrections being introduced (Charuchittipan et al., 2014; De Roo et al., 2018; Mauder et al., 2020)

Finally, the simplified schematizing of the air parcel exchange and coherent structures in SR and how they are related to mass and energy transport still provides open questions. Similarly, the role of different eddy sizes such as flux-bearing and non-flux-bearing remains debated (Shapland et al., 2012a,b; Suvočarev et al., 2014). On similar lines, the assumption in the ramp detection schemes (Van Atta, 1977; Chen et al., 1997a) and contribution of low frequency variance is not fully resolved. Further research in FV and SR may thus benefit from targeted large eddy simulations (Bailey and Stoll, 2016) to verify as well as visualize the analyzed relations and connections of coherent structures to surface fluxes, as done for instance for examining the widely known MOST relations (Maronga, 2014; Maronga and Reuder, 2017).

As shown here, by combining the FV and SR methods, H can be predicted reasonably. This is not the case for u_* and the associated stability parameter ξ. This finding can be explained by the different sensitivity of H and u_* on ξ and the fact that H in a wide range of unstable conditions can be estimated by its free convection limits (i.e. independent of u_*) while close to neutral conditions when the errors in u_* and ξ may be large a, σ_T and thus H are small. The inability to predict u_* along ξ without wind velocity measurements contradicts the original expectations of Tillman (1972) who attempted to estimate u_* from temperature variance and skewness. Nevertheless, the ability to predict H in this instrumentally simple manner is appealing given its wide applicability in studies assessing the surface energy fluxes including evapotranspiration as a residual of the energy balance budget (Kustas et al., 1994; Snyder et al., 1996). In the following studies, it is worth exploring whether it is possible to optimize the parameters involved in FV and SR to estimate H, u_* and L_O simultaneously.

6. Conclusions and future recommendations

FV and SR were evaluated against EC measurements at aerodynamically distinct surfaces that span a planar homogeneous ASL to a heterogeneous RSL. For SR, several different methods were tested. The methods cross-comparison suggested that the previous SR approaches relying on constant α parameter lack general support due to high

dependence of α on atmospheric stability. The study also did not prove the general validity of the two-scale VA approach relying on hypothesis of non-flux-bearing and flux-bearing coherent structures and suggests that the free convection approximation provides the most reliable H estimates from the list of previously provided SR methods relying only on high-frequency temperature measurements. The derivation (Eq. (27)) originally proposed by Castellví (2004) proved to be the most reliable across the sites. Due to previous criticism of combining SR and MOST, this derivation was revisited by employing a different set of assumptions and new perspective on the coordination between micro-and macro-scales.

Another new approach based on a combination of FV and SR was also derived (Eqs. (42) and (43)) allowing for reliable estimates of H (Eqs. (6) and (38) whose individual results can be either taken separately or averaged) with only a fast response thermocouple sensor. This approach is largely minimizing the need for the so-called alpha calibration and proved to be most reliable from the list of SR methods relying solely on the single point high-frequency temperature measurements. Moreover, the performance of this combined FV-SR approach was commensurate with the FV and SR methods that require estimates of u_* and L_O to be externally supplied by EC or an iterative method using additional wind speed measurements.

Finally, the study also shows that both FV and SR are sensitive to the choice of MOST universal function with SR being less sensitive to this choice. As in any MOST dependent methods, the choice of stability correction functions should be considered in future evaluations and special attention must be paid if the methods are applied under conditions of free convection when not all MOST parameterization are appropriate.

Moving forward, testing the methods across a wide range of environmental conditions and biomes such as FLUXNET (Baldocchi et al., 2001) would be a next logical step. This step would enable generality in the proposed relations here as well as it may contribute to new gap-filling schemes using FV and SR approaches (Guo et al., 2009).

Connections to other methods dependent on MOST such as scintillometry (Van Kesteren et al., 2013; Kooijmans and Hartogensis, 2016) are also timely. The reason is not only to have an alternative method to quantify surface fluxes with potentially lower costs (Pozníková et al., 2018), but mainly to elucidate the space–time relations embedded in the raw EC data. These relations have the potential to increase understanding so as to progress on practical problems such as the energy balance closure, the role of large eddies in the energy transport, and turbulent exchange in general (Lumley and Yaglom, 2001; Mauder et al., 2020; Liu et al., 2021).

Finally, employing a multi-tool assessment of surface energy fluxes is preferred since a convergence or divergence of the results from differing methods is of high diagnostic value and stimulates further research into the fundamentals of micrometeorology.

CRediT authorship contribution statement

Milan Fischer: Conceptualization, Methodology, Data curation, Formal analysis, Investigation, Writing — original draft, Writing – review & editing. **Gabriel Katul:** Conceptualization, Methodology, Investigation, Funding acquisition, Writing – original draft, Writing – review & editing. **Asko Noormets:** Conceptualization, Methodology, Writing – original draft, Funding acquisition. **Gabriela Pozníková:** Data curation, Methodology, Investigation, Writing – original draft. **Jean-Christophe Domec:** Methodology, Writing – original draft, Funding acquisition. **Matěj Orság:** Data curation, Methodology, Writing – original draft. **Zdeněk Žalud:** Project administration, Funding acquisition. **Miroslav Trnka:** Supervision, Funding acquisition. **John S. King:** Conceptualization, Supervision, Funding acquisition, Writing – original draft.

Declaration of competing interest

The authors declare that they have no known competing financial interests or personal relationships that could have appeared to influence the work reported in this paper.

Data availability

Data will be made available on request.

Acknowledgments

The study was conducted with support from the SustES, Czech Republic — "Adaptation strategies for sustainable ecosystem services and food security under adverse environmental conditions" (CZ.02.1.01/0.0/0.0/16_019/0000797) and by USDA NIFA-AFRI, USA Sustainable Bioenergy grant number 2011-67009-20089 "Loblolly pine-switch grass intercropping for sustainable timber and biofuels production in the Southeastern United States". The work by Gabriel Katul was supported by the U.S. National Science Foundation (NSF-AGS-2028633 and NSF-IOS-1754893) and by the Department of Energy, USA (No. DE-SC0022072/DE-SC0023309). A subset of R codes related to the analyses presented in this study is available at https://github.com/MilanFischer/FV-SR_methods.

Appendix A. Supplementary data

Supplementary material associated with this article can be found, in the online version, at https://doi.org/10.1016/j.agrformet.2023.109692.

References

Albertson, J.D., Parlange, M.B., Katul, G.G., Chu, C.-R., Stricker, H., Tyler, S., 1995. Sensible heat flux From Arid Regions: A simple flux-variance method. Water Resour. Res. 31 (4), 969–973.

Ardia, D., Boudt, K., Carl, P., Mullen, K., Peterson, B., 2011. Differential evolution with DEoptim. R J. 3 (1), 27.

Aubinet, M., Grelle, A., Ibrom, A., Rannik, Ü., Moncrieff, J., Foken, T., Kowalski, A.S., Martin, P.H., Berbigier, P., Bernhofer, C., Clement, R., Elbers, J., Granier, A., Grünwald, T., Morgenstern, K., Pilegaard, K., Rebmann, C., Snijders, W., Valentini, R., Vesala, T., 1999. Estimates of the annual net carbon and water exchange of forests: The EUROFLUX methodology. In: Fitter, A., Raffaelli, D. (Eds.), Advances in Ecological Research, Vol. 30. Academic Press, pp. 113–175.

Bailey, B.N., Stoll, R.D., 2016. The creation and evolution of coherent structures in plant canopy flows and their role in turbulent transport. J. Fluid Mech. 789, 425–460.

Baldocchi, D., Falge, E., Gu, L., Olson, R., Hollinger, D., Running, S., Anthoni, P., Bernhofer, C., Davis, K., Evans, R., Fuentes, J., Goldstein, A., Katul, G., Law, B., Lee, X., Malhi, Y., Meyers, T., Munger, W., Oechel, W., U, K.T.P., Pilegaard, K., Schmid, H.P., Valentini, R., Verma, S., Vesala, T., Wilson, K., Wofsy, S., 2001. FLUXNET: A new tool to study the temporal and spatial variability of ecosystem-scale carbon dioxide, water vapor, and energy flux densities. Bull. Am. Meteorol. Soc. 82 (11), 2415–2434.

Barthlott, C., Drobinski, P., Fesquet, C., Dubos, T., Pietras, C., 2007. Long-term study of coherent structures in the atmospheric surface layer. Bound.-Lay. Meteorol. 125 (1), 1–24.

Beljaars, A.C.M., Holtslag, A.A.M., 1991. Flux parameterization over land surfaces for atmospheric models. J. Appl. Meteorol. Climatol. 30 (3), 327–341.

Berkowicz, R., Prahm, L.P., 1979. Generalization of k theory for turbulent diffusion. Part I: Spectral turbulent diffusivity concept. J. Appl. Meteorol. (1962-1982) 18 (3), 266–272.

Brunet, Y., 2020. Turbulent flow in plant canopies: historical perspective and overview. Bound.-Lay. Meteorol. 177 (2), 315–364.

Brunet, Y., Irvine, M.R., 2000. The control of coherent eddies in vegetation canopies: Streamwise structure spacing, canopy shear scale and atmospheric stability. Bound.-Lay. Meteorol. 94 (1), 139–163.

Brutsaert, W., 1965. A model for evaporation as a molecular diffusion process into a turbulent atmosphere. J. Geophys. Res. (1896-1977) 70 (20), 5017–5024.

Castellví, F., 2004. Combining surface renewal analysis and similarity theory: A new approach for estimating sensible heat flux. Water Resour. Res. 40, W05201.

Castellvi, 2007. The estimation of latent heat flux: A reflection for the future. Tethys, J. Weather Clim. West. Mediterr..

Castellví, F., 2013. A method for estimating the sensible heat flux in the inertial sublayer from high-frequency air temperature and averaged gradient measurements. Agricult. Forest Meteorol. 180, 68–75.
Castellví, F., Cammalleri, C., Ciraolo, G., Maltese, A., Rossi, F., 2016. Daytime sensible heat flux estimation over heterogeneous surfaces using multitemporal land-surface temperature observations. Water Resour. Res. 52, 3457–3476.
Castellví, F., Consoli, S., Papa, R., 2012. Sensible heat flux estimates using two different methods based on surface renewal analysis. a study case over an orange orchard in Sicily. Agricult. Forest Meteorol. 152, 58–64.
Castellví, F., Perez, P.J., Ibañez, M., 2002. A method based on high-frequency temperature measurements to estimate the sensible heat flux avoiding the height dependence. Water Resour. Res. 38 (6), 20–1–20–9.
Castellví, F., Snyder, R.L., 2009. Combining the dissipation method and surface renewal analysis to estimate scalar fluxes from the time traces over rangeland grass near Ione (California). Hydrol. Process. 23 (6), 842–857.
Castellví, F., Snyder, R.L., 2010. A comparison between latent heat fluxes over grass using a weighing lysimeter and surface renewal analysis. J. Hydrol. 381 (3–4), 213–220.
Castellví, F., Snyder, R.L., Baldocchi, D.D., 2008. Surface energy-balance closure over rangeland grass using the eddy covariance method and surface renewal analysis. Agricult. Forest Meteorol. 148 (6–7), 1147–1160.
Castellví, F., Snyder, R.L., Baldocchi, D.D., Martí nez Cob, A., 2006. A comparison of new and existing equations for estimating sensible heat flux using surface renewal and similarity concepts. Water Resour. Res. 42 (8).
Cava, D., Katul, G.G., Scrimieri, A., Poggi, D., Cescatti, A., Giostra, U., 2006. Buoyancy and the sensible heat flux budget within dense canopies. Bound.-Lay. Meteorol. 118 (1), 217–240.
Cellier, P., Brunet, Y., 1992. Flux-gradient relationships above tall plant canopies. Agricult. Forest Meteorol. 58 (1), 93–117.
Charuchittipan, D., Babel, W., Mauder, M., Leps, J.-P., Foken, T., 2014. Extension of the averaging time in eddy-covariance measurements and its effect on the energy balance closure. Bound.-Lay. Meteorol. 152 (3), 303–327.
Chasmer, L., Kljun, N., Hopkinson, C., Brown, S., Milne, T., Giroux, K., Barr, A., Devito, K., Creed, I., Petrone, R., 2011. Characterizing vegetation structural and topographic characteristics sampled by eddy covariance within two mature aspen stands using lidar and a flux footprint model: Scaling to MODIS. J. Geophys. Res. Biogeosci. 116 (G2).
Chen, W., Novak, M.D., Black, T.A., Lee, X., 1997a. Coherent eddies and temperature structure functions for three contrasting surfaces. Part I: Ramp model with finite microfront time. Bound.-Lay. Meteorol. 84 (1), 99–124.
Chen, W., Novak, M.D., Black, T.A., Lee, X., 1997b. Coherent eddies and temperature structure functions for three contrasting surfaces. Part II: Renewal model for sensible heat flux. Bound.-Lay. Meteorol. 84 (1), 125–147.
Chenge, Y., Brutsaert, W., 2005. Flux-profile relationships for wind speed and temperature in the stable atmospheric boundary layer. Bound.-Lay. Meteorol. 114 (3), 519–538.
Collineau, S., Brunet, Y., 1993a. Detection of turbulent coherent motions in a forest canopy part I: Wavelet analysis. Bound.-Lay. Meteorol. 65 (4), 357–379.
Collineau, S., Brunet, Y., 1993b. Detection of turbulent coherent motions in a forest canopy part II: Time-scales and conditional averages. Bound.-Lay. Meteorol. 66 (1), 49–73.
Crank, J., 1975. The Mathematics of Diffusion. In: Oxford science publications, Clarendon Press.
Davy, R., Davis, J.A., Taylor, P.A., Lange, C.F., Weng, W., Whiteway, J., Gunnlaugson, H.P., 2010. Initial analysis of air temperature and related data from the phoenix MET station and their use in estimating turbulent heat fluxes. J. Geophys. Res. Planets 115 (E3).
De Bruin, H.A.R., Hartogensis, O.K., 2005. Variance method to determine turbulent fluxes of momentum and sensible heat in the stable atmospheric surface layer. Bound.-Lay. Meteorol. 116 (2), 385–392.
De Bruin, H.A.R., Kohsiek, W., Van Den Hurk, B.J.J.M., 1993. A verification of some methods to determine the fluxes of momentum, sensible heat, and water vapour using standard deviation and structure parameter of scalar meteorological quantities. Bound.-Lay. Meteorol. 63 (3), 231–257.
De Ridder, K., 2010. Bulk transfer relations for the roughness sublayer. Bound.-Lay. Meteorol. 134 (2), 257–267.
De Roo, F., Zhang, S., Huq, S., Mauder, M., 2018. A semi-empirical model of the energy balance closure in the surface layer. PLoS One 13 (12), e0209022.
Dias, N.L., Chamecki, M., Kan, A., Okawa, C.M.P., 2004. A study of spectra, structure and correlation functions and their implications for the stationarity of surface-layer turbulence. Bound.-Lay. Meteorol. 110 (2), 165–189.
Drexler, J.Z., Snyder, R.L., Spano, D., Paw U, K.T., 2004. A review of models and micrometeorological methods used to estimate wetland evapotranspiration. Hydrol. Process. 18 (11), 2071–2101.
Duce, P., Spano, D., Snyder, R., Paw, U., 1998. Effect of different fine-wire thermocouple design on high frequency temperature measurement. In: AMS 23rd Conference on Agricultural and Forest Meteorology. Albuquerque, NM, pp. 2–6.
Foken, T., 2008a. Micrometeorology. Springer-Verlag, Berlin, Heidelberg.
Foken, T., 2008b. The energy balance closure problem: An overview. Ecol. Appl. 18, 1351–1367.
Foken, T., Skeib, G., Richter, S., 1991. Dependence of the integral turbulence characteristics on the stability of stratification and their use for Doppler-sodar measurements. Meteorol. Z. 41 (4), 311–315.
French, A.N., Alfieri, J.G., Kustas, W.P., Prueger, J.H., Hipps, L.E., Chávez, J.L., Evett, S.R., Howell, T.A., Gowda, P.H., Hunsaker, D.J., Thorp, K.R., 2012. Estimation of surface energy fluxes using surface renewal and flux variance techniques over an advective irrigated agricultural site. Adv. Water Resour. 50, 91–105.
Gao, F., Anderson, M., Daughtry, C., Karnieli, A., Hively, D., Kustas, W., 2020. A within-season approach for detecting early growth stages in corn and soybean using high temporal and spatial resolution imagery. Remote Sens. Environ. 242, 111752.
Gao, W., Shaw, R.H., Paw U, K.T., 1989. Observation of organized structure in turbulent flow within and above a forest canopy. In: Boundary Layer Studies and Applications. Springer, pp. 349–377.
Ghannam, K., Duman, T., Salesky, S.T., Chamecki, M., Katul, G., 2017. The non-local character of turbulence asymmetry in the convective atmospheric boundary layer. Q. J. R. Meteorol. Soc. 143 (702), 494–507.
Grachev, A.A., Andreas, E.L., Fairall, C.W., Guest, P.S., Persson, P.O.G., 2007. SHEBA flux–profile relationships in the stable atmospheric boundary layer. Bound.-Lay. Meteorol. 124 (3), 315–333.
Grachev, A.A., Fairall, C.W., Bradley, E.F., 2000. Convective profile constants revisited. Bound.-Lay. Meteorol. 94 (3), 495–515.
Gray, B.A., Toucher, M.L., Savage, M.J., Clulow, A.D., 2022. Seasonal evapotranspiration over an invader vegetation (*Pteridium aquilinum*) in a degraded montane grassland using surface renewal. J. Hydrol. Region. Stud. 40, 101012.
Guo, X., Zhang, H., Cai, X., Kang, L., Zhu, T., Leclerc, M.Y., 2009. Flux-variance method for latent heat and carbon dioxide fluxes in unstable conditions. Bound.-Lay. Meteorol. 131 (3), 363–384.
Hall, R.L., 2002. Aerodynamic resistance of coppiced poplar. Agricult. Forest Meteorol. 114 (1), 83–102.
Higbie, R., 1935. The rate of adsorption of a pure gas into a still liquid during short periods of exposure. Trans. Am. Inst. Chem. Eng. 31 (2), 365–389.
Högström, U., 1988. Non-dimensional wind and temperature profiles in the atmospheric surface layer: A re-evaluation. Bound.-Lay. Meteorol. 42 (1), 55–78.
Holwerda, F., Guerrero-Medina, O., Meesters, A.G.C.A., 2021. Evaluating surface renewal models for estimating sensible heat flux above and within a coffee agroforestry system. Agricult. Forest Meteorol. 308–309, 108598.
Hsieh, C.-I., Katul, G.G., 1997. Dissipation methods, taylor's hypothesis, and stability correction functions in the atmospheric surface layer. J. Geophys. Res.: Atmos. 102 (D14), 16391–16405.
Hsieh, C.-I., Katul, G.G., Schieldge, J., Sigmon, J., Knoerr, K.R., 1996. Estimation of momentum and heat fluxes using dissipation and flux-variance methods in the unstable surface layer. Water Resour. Res. 32 (8), 2453–2462.
Hsieh, C.-I., Lai, M.-C., Hsia, Y.-J., Chang, T.-J., 2008. Estimation of sensible heat, water vapor, and CO_2 fluxes using the flux-variance method. Int. J. Biometeorol. 52 (6), 521–533.
Jackson, P., 1981. On the displacement height in the logarithmic velocity profile. J. Fluid Mech. 111, 15–25.
Kader, B., Yaglom, A., 1990. Mean fields and fluctuation moments in unstably stratified turbulent boundary layers. J. Fluid Mech. 212, 637–662.
Kaimal, J.C., Finnigan, J.J., 1994. Atmospheric Boundary Layer Flows. Oxford University Press, New York.
Katul, G.G., Geron, C.D., Hsieh, C.-I., Vidakovic, B., Guenther, A.B., 1998a. Active turbulence and scalar transport near the forest–atmosphere interface. J. Appl. Meteorol. 37 (12), 1533–1546.
Katul, G.G., Geron, C.D., Hsieh, C.-I., Vidakovic, B., Guenther, A.B., 1998b. Active turbulence and scalar transport near the forest–atmosphere interface. J. Appl. Meteorol. 37 (12), 1533–1546.
Katul, G., Goltz, S.M., Hsieh, C.-I., Cheng, Y., Mowry, F., Sigmon, J., 1995. Estimation of surface heat and momentum fluxes using the flux-variance method above uniform and non-uniform terrain. Bound.-Lay. Meteorol. 74 (3), 237–260.
Katul, G., Hiseh, C.-I., Sigmon, J., 1997. Energy-inertial scale interactions for velocity and temperature in the unstable atmospheric surface layer. Bound.-Lay. Meteorol. 82 (1), 49–80.
Katul, G., Hsieh, C.-I., Oren, R., Ellsworth, D., Phillips, N., 1996. Latent and sensible heat flux predictions from a uniform pine forest using surface renewal and flux variance methods. Bound.-Lay. Meteorol. 80 (3), 249–282.
Katul, G., Liu, H., 2017. A Kolmogorov-Brutsaert structure function model for evaporation into a turbulent atmosphere. Water Resour. Res. 53 (5), 3635–3644.
Katul, G., Vidakovic, B., 1996. The partitioning of attached and detached eddy motion in the atmospheric surface layer using Lorentz wavelet filtering. Bound.-Lay. Meteorol. 77 (2), 153–172.
Kljun, N., Calanca, P., Rotach, M.W., Schmid, H.P., 2015. A simple two-dimensional parameterisation for Flux Footprint Prediction (FFP). Geosci. Model Dev. 8 (11), 3695–3713.
Kooijmans, L.M.J., Hartogensis, O.K., 2016. Surface-layer similarity functions for dissipation rate and structure parameters of temperature and humidity based on eleven field experiments. Bound.-Lay. Meteorol. 160 (3), 501–527.
Kotani, A., Sugita, M., 2007. Variance methods to estimate regional heat fluxes with aircraft measurements in the convective boundary layer. J. Hydrol. 333 (1), 68–85.

Kustas, W.P., Blanford, J.H., Stannard, D.I., Daughtry, C.S.T., Nichols, W.D., Weltz, M.A., 1994. Local energy flux estimates for unstable conditions using variance data in semiarid rangelands. Water Resour. Res. 30 (5), 1351–1361.

Laubach, J., McNaughton, K.G., Wilson, J.D., 2000. Heat and water vapour diffusivities near the base of a disturbed stable internal boundary layer. Bound.-Lay. Meteorol. 94, 23–63.

Lindroth, A., Halldin, S., 1990. Gradient measurements with fixed and reversing temperature and humidity sensors above a thin forest. Agricult. Forest Meteorol. 53 (1), 81–103.

Liu, H., Gao, Z., Katul, G.G., 2021. Non-closure of surface energy balance linked to asymmetric turbulent transport of scalars by large eddies. J. Geophys. Res.-Atmos. 126 (7), e2020JD034474.

Lloyd, C.R., Culf, A.D., Dolman, A.J., Gash, J.H.C., 1991. Estimates of sensible heat flux from observations of temperature fluctuations. Bound.-Lay. Meteorol. 57 (4), 311–322.

Lumley, J.L., Yaglom, A.M., 2001. A century of turbulence. Flow Turbul. Combust. 66 (3), 241–286.

Maronga, B., 2014. Monin–obukhov similarity functions for the structure parameters of temperature and humidity in the unstable surface layer: results from high-resolution large-eddy simulations. J. Atmos. Sci. 71, 716–733.

Maronga, B., Reuder, J., 2017. On the formulation and universality of monin–obukhov similarity functions for mean gradients and standard deviations in the unstable surface layer: results from surface-layer-resolving large-eddy simulations. J. Atmos. Sci. 74, 989–1010.

Mauder, M., Foken, T., Cuxart, J., 2020. Surface-energy-balance closure over land: A review. Bound.-Lay. Meteorol. 177 (2), 395–426.

Mekhmandarov, Y., Pirkner, M., Achiman, O., Tanny, J., 2015. Application of the surface renewal technique in two types of screenhouses: Sensible heat flux estimates and turbulence characteristics. Agricult. Forest Meteorol. 203, 229–242.

Meyers, T., Paw U, K.T., 1986. Testing of a higher-order closure model for modeling airflow within and above plant canopies. Bound.-Lay. Meteorol. 37 (3), 297–311.

Miao, G., Noormets, A., Domec, J.-C., Fuentes, M., Trettin, C.C., Sun, G., McNulty, S.G., King, J.S., 2017. Hydrology and microtopography control carbon dynamics in wetlands: Implications in partitioning ecosystem respiration in a coastal plain forested wetland. Agricult. Forest Meteorol. 247, 343–355.

Mölder, M., Grelle, A., Lindroth, A., Halldin, S., 1999. Flux-profile relationships over a boreal forest — roughness sublayer corrections. Agricult. Forest Meteorol. 98–99, 645–658.

Monin, A.S., Obukhov, A.M.F., 1954. Osnovnye zakonomernosti turbulentnogo peremeshivanija v prizemnom sloe atmosfery (Basic laws of turbulent mixing in the surface layer of the atmosphere), Vol. 151. Trudy Geofizicheskogo Instituta Akademiya Nauk SSSR, pp. 163–187.

Moog, D.B., Jirka, G.H., 1999. Air-water gas transfer in uniform channel flow. J. Hydraul. Eng. 125 (1), 3–10.

Obukhov, A.M., 1946. Turbulentnost' v temperaturnoj - neodnorodnoj atmosfere (Turbulence in an atmosphere with a non-uniform temperature), Vol. 1. Trudy Geofizicheskogo Instituta, Akademiya Nauk SSSR, pp. 95–115.

Pahlow, M., Parlange, M.B., Porté-Agel, F., 2001. On Monin–Obukhov similarity in the stable atmospheric boundary layer. Bound.-Lay. Meteorol. 99 (2), 225–248.

Paulson, C., 1970. The mathematical representation of wind speed and temperature profiles in the unstable atmospheric surface layer. J. Appl. Meteorol. Climatol. 9 (6), 857–861.

Paw U, K.T., Brunet, Y., 1991. A surface renewal measure of sensible heat flux density. In: 20. Agricultural and Forest Meteorology Conference. AMS-American Meteorological Society, pp. 52–53.

Paw U, K.T., Brunet, Y., Collineau, S., Shaw, R.H., Maitani, T., Qiu, J., Hipps, L., 1992. On coherent structures in turbulence above and within agricultural plant canopies. Agricult. Forest Meteorol. 61 (1–2), 55–68.

Paw U, K.T., Qiu, J., Su, H.-B., Watanabe, T., Brunet, Y., 1995. Surface renewal analysis: a new method to obtain scalar fluxes. Agricult. Forest Meteorol. 74, 119–137.

Paw U, K.T., Snyder, R.L., Spano, D., Hong-Bing, S., 2005. Surface renewal estimates of scalar exchange. Refereed chapter in micrometeorology of agricultural systems. In: Hatfield, J.L. (Ed.), Agronomy Society of America. Madison, pp. 455–483.

Poggi, D., Porporato, A., Ridolfi, L., Albertson, J.D., Katul, G.G., 2004. The effect of vegetation density on canopy sub-layer turbulence. Bound.-Lay. Meteorol. 111 (3), 565–587.

Pope, S.B., 2000. Turbulent Flows. Cambridge University Press, p. 734.

Pozníková, G., Fischer, M., van Kesteren, B., Orság, M., Hlavinka, P., Žalud, Z., Trnka, M., 2018. Quantifying turbulent energy fluxes and evapotranspiration in agricultural field conditions: A comparison of micrometeorological methods. Agricult. Water Manag. 209, 249–263.

Priestley, C.H.B., 1959. Turbulent Transfer in the Lower Atmosphere. University of Chicago Press.

Qiu, J., Paw U, K.T., Shaw, R.H., 1995. Pseudo-wavelet analysis of turbulence patterns in three vegetation layers. Bound.-Lay. Meteorol. 72 (1), 177–204.

R Core Team, 2023. R: A language and environment for statistical computing.

Raupach, M.R., 1989. A practical Lagrangian method for relating scalar concentrations to source distributions in vegetation canopies. Q. J. R. Meteorol. Soc. 115 (487), 609–632.

Raupach, M.R., Finnigan, J.J., Brunei, Y., 1996. Coherent eddies and turbulence in vegetation canopies: The mixing-layer analogy. Bound.-Lay. Meteorol. 78 (3), 351–382.

Raupach, M.R., Thom, A.S., 1981. Turbulence in and above plant canopies. Annu. Rev. Fluid Mech. 13 (1), 97–129.

Raupach, M.R., Thom, A.S., Edwards, I., 1980. A wind-tunnel study of turbulent flow close to regularly arrayed rough surfaces. Bound.-Lay. Meteorol. 18 (4), 373–397.

Rosa, R., Dicken, U., Tanny, J., 2013. Estimating evapotranspiration from processing tomato using the surface renewal technique. Biosystems Engineering 114 (4), 406–413.

Rosa, R., Tanny, J., 2015. Surface renewal and eddy covariance measurements of sensible and latent heat fluxes of cotton during two growing seasons. Biosyst. Eng. 136, 149–161.

Roussel, J.-R., Auty, D., Coops, N.C., Tompalski, P., Goodbody, T.R.H., Meador, A.S., Bourdon, J.-F., Boissieu, F.d., Achim, A., 2020. lidR: An R package for analysis of Airborne Laser Scanning (ALS) data. Remote Sens. Environ. 251, 112061.

Schotanus, P., Nieuwstadt, F., De Bruin, H., 1983. Temperature measurement with a sonic anemometer and its application to heat and moisture fluxes. Bound.-Lay. Meteorol. 26 (1), 81–93.

Sfyri, E., Rotach, M.W., Stiperski, I., Bosveld, F.C., Lehner, M., Obleitner, F., 2018. Scalar-flux similarity in the layer near the surface over mountainous terrain. Bound.-Lay. Meteorol. 169 (1), 11–46.

Shapland, T.M., McElrone, A.J., Snyder, R.L., Paw U, K.T., 2012a. Structure function analysis of two-scale scalar ramps. Part I: Theory and modelling. Bound.-Lay. Meteorol. 145, 5–25.

Shapland, T.M., McElrone, A.J., Snyder, R.L., Paw U, K.T., 2012b. Structure function analysis of two-scale scalar ramps. Part II: Ramp characteristics and surface renewal flux estimation. Bound.-Lay. Meteorol. 145, 27–44.

Shapland, T.M., Snyder, R.L., Paw U, K.T., McElrone, A.J., 2014. Thermocouple frequency response compensation leads to convergence of the surface renewal alpha calibration. Agricult. Forest Meteorol. 189–190, 36–47.

Shapland, T.M., Snyder, R.L., Smart, D.R., Williams, L.E., 2012c. Estimation of actual evapotranspiration in winegrape vineyards located on hillside terrain using surface renewal analysis. Irrigation Sci. 30 (6), 471–484.

Shaw, R.H., Pereira, A.R., 1982. Aerodynamic roughness of a plant canopy: A numerical experiment. Agric. Meteorol. 26 (1), 51–65.

Shuttleworth, W.J., 2007. Putting the "vap" into evaporation. Hydrol. Earth Syst. Sci. 11, 210–244.

Siqueira, M., Katul, G., 2002. Estimating heat sources and fluxes in thermally stratified canopy flows using higher-order closure models. Bound.-Lay. Meteorol. 103 (1), 125–142.

Snyder, R.L., Spano, D., Duce, P., Baldocchi, D., Xu, L., Paw U, K.T., 2006. A fuel dryness index for grassland fire-danger assessment. Agricult. Forest Meteorol. 139 (1–2), 1–11.

Snyder, R.L., Spano, D., Pawu, K.T., 1996. Surface renewal analysis for sensible and latent heat flux density. Bound.-Lay. Meteorol. 77 (3), 249–266.

Sorbjan, Z., 1987. An examination of local similarity theory in the stably stratified boundary layer. Bound.-Lay. Meteorol. 38 (1), 63–71.

Sorbjan, Z., 1989. Structure of the Atmospheric Boundary Layer. Prentice Hall, Englewood Cliffs, New Jersey, USA.

Spano, D., Snyder, R.L., Duce, P., Paw U, K.T., 1997. Surface renewal analysis for sensible heat flux density using structure functions. Agricult. Forest Meteorol. 86 (3), 259–271.

Spano, D., Snyder, R.L., Duce, P., Paw U, K.T., 2000. Estimating sensible and latent heat flux densities from grapevine canopies using surface renewal. Agricult. Forest Meteorol. 104 (3), 171–183.

Stannard, D.I., 1997. A theoretically based determination of Bowen-ratio fetch requirements. Bound.-Lay. Meteorol. 83 (3), 375–406.

Stull, R.B., 1988. An Introduction To Boundary Layer Meteorology. Springer.

Sutton, O., 1953. Micrometeorology: A Study of Physical Processes in the Lowest Layers of the Earth's Atmosphere. McGraw-Hill, p. 333.

Suvočarev, K., Castellví, F., Reba, M.L., Runkle, B.R.K., 2019. Surface renewal measurements of H, λE and CO_2 fluxes over two different agricultural systems. Agricult. Forest Meteorol. 279, 107763.

Suvočarev, K., Shapland, T.M., Snyder, R.L., Martínez-Cob, A., 2014. Surface renewal performance to independently estimate sensible and latent heat fluxes in heterogeneous crop surfaces. J. Hydrol. 509, 83–93.

Thom, A.S., Stewart, J.B., Oliver, H.R., Gash, J.H.C., 1975. Comparison of aerodynamic and energy budget estimates of fluxes over a pine forest. Q. J. R. Meteorol. Soc. 101 (427), 93–105.

Thomas, C., Foken, T., 2006. Organised motion in a tall spruce canopy: Temporal scales, structure spacing and terrain effects. Bound.-Lay. Meteorol. 122 (1), 123–147.

Tian, S., Cacho, J.F., Youssef, M.A., Chescheir, G.M., Fischer, M., Nettles, J.E., King, J.S., 2017. Switchgrass growth and pine–switchgrass interactions in established intercropping systems. GCB Bioenergy 9 (5), 845–857.

Tillman, J.E., 1972. The indirect determination of stability, heat and momentum fluxes in the atmospheric boundary layer from simple scalar variables during dry unstable conditions. J. Appl. Meteorol. Climatol. 11 (5), 783–792.

Torrence, C., Compo, G.P., 1998. A practical guide to wavelet analysis. Bull. Am. Meteorol. Soc. 79 (1), 61–78.

Van Atta, C., 1977. Effect of coherent structures on structure functions of temperature in the atmospheric boundary layer. Arch. Mech. 29 (1), 161–171.
Van Atta, C.W., 1978. Coherent structure ramp models for structure functions of temperature in turbulent shear flows. In: Fiedler, H. (Ed.), Structure and Mechanisms of Turbulence II. Springer Berlin Heidelberg, Berlin, Heidelberg, pp. 138–153.
Van Kesteren, B., Hartogensis, O., van Dinther, D., Moene, A., De Bruin, H., 2013. Measuring H_2O and CO_2 fluxes at field scales with scintillometry: Part I – introduction and validation of four methods. Agricult. Forest Meteorol. 178–179, 75–87.
Verhoef, A., Mcnaughton, K.G., Jacobs, A.F.G., 1997. A parameterization of momentum roughness length and displacement height for a wide range of canopy densities. Hydrol. Earth Syst. Sci. Discuss. 1 (1), 81–91.
Wang, J., Bras, R.L., 1998. A new method for estimation of sensible heat flux from air temperature. Water Resour. Res. 34 (9), 2281–2288.
Warhaft, Z., 2000. Passive scalars in turbulent flows. Annu. Rev. Fluid Mech. 32 (1), 203–240.
Waterman, T., Bragg, A.D., Katul, G., Chaney, N., 2022. Examining parameterizations of potential temperature variance across varied landscapes for use in earth system models. J. Geophys. Res.: Atmos. 127 (8), e2021JD036236.
Weaver, H.L., 1990. Temperature and humidity flux-variance relations determined by one-dimensional eddy correlation. Bound.-Lay. Meteorol. 53 (1), 77–91.
Wesely, M.L., 1988. Use of variance techniques to measure dry air-surface exchange rates. Bound.-Lay. Meteorol. 44 (1), 13–31.
Wesson, K.H., Katul, G., Lai, C.-T., 2001. Sensible heat flux estimation by flux variance and half-order time derivative methods. Water Resour. Res. 37 (9), 2333–2343.
Zeri, M., Sá, L.D.A., Nobre, C.A., 2013. Estimating buoyancy heat flux using the surface renewal technique over four amazonian forest sites in Brazil. Bound.-Lay. Meteorol. 149 (2), 179–196.